CALCULATION OF TOTAL AND ONE-NUCLEON REMOVAL CROSS SECTIONS USING THE GLAUBER MODEL

BY

IBRAHIM SA'ADU
(SPS/12/MPY/00031)
B.Sc. PHYSICS

A DISSERTATION SUBMITTED TO THE DEPARTMENT OF PHYSICS, BAYERO UNIVERSITY KANO, IN PARTIAL FULFILMENT OF THE REQUIREMENTS FOR THE AWARD OF DEGREE OF MASTER OF SCIENCE (M.Sc.) IN PHYSICS.

SEPTEMBER, 2016

DECLARATION

I hereby declare that this project is the result of my research work and to the best of my knowledge no part of the contents had been used in a previous application for higher qualification. All sources of knowledge utilized have been duly acknowledged.

……. …….

Ibrahim Sa'adu Date
SPS/12/MPY/00031

CERTIFICATION

This is to certify that the research work for this thesis and the succeeding preparation by (Ibrahim Sa'adu) with registration number (SPS/12/MPY/00031) were carried out under my supervision.

…….……. ……
Dr. I. D. Adamu Date
(Supervisor)

……. ….……...
Dr. T. H. Darma Date
(Head of Department)

APPROVAL PAGE

This is to certify that this thesis titled Calculation of Total and One-Nucleon Removal Cross Section by Ibrahim Sa'adu, has met the requirement of the rules governing the award of Degree of Master of Science (M.Sc.) in Physics, Bayero University Kano and is approved for the contribution to knowledge and literary presentation.

……. ……..……..

Prof. J. O. Fiase Date
(External Examiner)

…….. ...…….

Dr. A. M. Nura Date
(Internal Examiner)

……. ……..……..

Dr. I. D. Adamu Date
(Supervisor)

……. …….

Dr. T. H. Darma Date
(Head of Department)

…….. …….

Dr. N. Hussaini Date
(SPS Representative)

ACKNOWLEDGMENT

In the name of Allah the Most Beneficent the Most Merciful. Praise be to Allah, Lord of the universe. Blessing and peace be upon our Prophet (S. A.W), his household, his companions and all those who follow his teaching till the day of judgment. I wish express my sincere gratitude to my parent for all they have been doing for me in my life, May Allah (S.W) reward them with Jannatul Firdaus. Also my appreciation goes to my wife Halima Muhammad who has been by my side always.

My appreciation and respect goes to my supervisor Dr. I. D. Adamu for the great assistance, guidance and support toward the conclusion of this work, most especially during computation work.Also my appreciation goes to the entire staff of Physics Department Bayero University Kano, especially Dr. A. S Gidado and Dr. A. M Nura for their advice and support.

My deepest appreciation goes to Alhaji Mika'ilu Buhari Birnin Yero for advice and supports both academically and financially.

Finally special thanks go to my brothers, sisters, uncles, aunties and friends, especially Idris Salisu Sani (Abba), Nasiru Sharehu, Nura Sharehu, Tukur Sharehu, Hafiz Sa'ad, Fatimatu Sa'ad, Zainab Sa'ad and Maharazu Sa'ad.

DEDICATION

ALHAJI MIKA’IL ALIYU BUHARI BIRNIN YERO (tetfund).

TABLE OF CONTENTS

ABSTRACT

In this work the elastic and inelastic cross sections, total and one-nucleon removal cross sections for the reaction systems **^{11}Be + ^{12}C, ^{13}C + ^{12}C, ^{19}C + ^{12}C** and**Mg^{37} + ^{12}C** were computed in the frame work of Glauber theory using the Cross Section Calculation in the Glauber Model (CSC_GM) program code. The CSC_GM code, which is a Fortran 90 program, was obtained from the Computer Physics Communication (CPC) Program Library, Queen's University of Belfast, Northern Ireland. The code was run on Linux operating system. The projectile nucleus is assumed to have the structure of a core plus valence nucleon. The result showed that both **^{11}Be, ^{19}C and ^{37}Mg** exhibit a halo structure, while **^{13}C** does not show any halo characteristic.

CHAPTER ONE (INTRODUCTION)

1.0 GENERAL INTRODUCTION

Nuclear reactions are some of the fundamental reactions in nature. Understanding nuclear reactions is important not only in nuclear physics but also in cosmology and astrophysics. The study of nuclear reactions is necessary to understand the mechanism of nucleosynthesis in the early universe, stellar evolution, and supernova explosions, and to eventually understand the origin of elements in the universe. Application of the study to nuclear engineering is another important direction (Yahiro *et al*., 2012). The theoretical study of scattering and reactions involving halo nuclei at the relatively high fragmentation beam energies at which so many of the experiment have been conducted, has led to a renaissance of a number of semi-classical reaction models. In particular, the Glauber model, which was first applied to nuclear scattering in the late 1950s, provides a remarkably simple framework for calculating various important observables arising from experiments involving loosely-bound projectiles such as halo nuclei. Its central assumption is the eikonal approximation (Abu-Ibahim, *et al*., 2002): that the projectile travels along a definite straight line trajectory through the field of the target nucleus allows for the derivation of a number of crucial yet simple cross section formulae (Al-khalili, 2004). The Glauber model is a microscopic reaction theory of high-energy collision based on the eikonal approximation and on the bare nucleon–nucleon interaction. It is now a standard tool to calculate the cross sections because it can account for a significant part of breakup effects which play an important role in the reaction of a weakly bound nucleus.

Experimental study of unstable nuclei has considerably advanced through the technique of using secondary radioactive beams. The quantities measured in the study include various inclusive cross sections, for example, reaction or interaction cross sections, differential cross section and nucleon-removal cross sections of a fragment. These quantities have played an important role to reveal the nuclear structure of unstable nuclei, particularly halo structure, proton and neutron skins (Adamu 2013). Halo and skin are nuclear properties that are common to only unstable radioactive nuclei.

1.1 NUCLEAR HALO AND SKIN

1.1.1 Nuclear Halo

Nuclear halo formation is an important feature of nuclei with extreme neutron to proton number asymmetry near the limits of nuclear stability. The halo, a dilute neutron or proton cloud of large radius, has a small spatial overlap with a core of more tightly bound nucleons. Necessary conditions for halo formation are that one or two valence neutrons have: (a) weak binding, with typical separation energies $Sn \prec 1$ MeV, which are significantly lower than the more conventional 8 MeV, and (b) low orbital angular momenta, $\ell = 0$ or 1. The reactions of nuclei with such spatially extended halo distributions lead to several interesting phenomena such as energy excitations, narrow momentum distributions of the core fragments following dissociation, reflecting low energy of the halo neutron(s) and large reaction cross sections (Sawhney *et al.,* 2014). An example is ^{11}Be consisting of a single neutron around a ^{10} Be core. The extra neutron has wave function with a rms radius of ~ 6 fm compared to the core radius of ~ 2.5 fm. Another example is ^{6}He consisting of two neutrons outside a ^{4}He core. This is an example

of a *Borromean nucleus* consisting of three objects that are bound, while the three possible pairs are unbound. In this case, ^{6}He is bound while n-n and n-^{4}He are unbound (Al-khalili 2004).

"Halo nuclei are very weakly-bound exotic states of nuclear matter in which the outer one or two valence nucleons (usually neutrons) are spatially decoupled from a relatively tightly bound core such that they spend more than half their time beyond the range of the binding nuclear potential. In this sense, the halo is a threshold phenomenon in which the halo nucleons quantum tunnel out to large distances, giving rise to extended wave function tails and hence large overall matter radii.

1.1.2 Nuclear Skin

Qualitatively, the term "nuclear skin" describes an excess of neutrons or protons at the nuclear surface, whereas "nuclear halo" stands for such excess plus a tail of the neutron or proton-density distribution. In other words, an excess of several neutrons or protons builds up so that the neutron or proton density actually extends out significantly further than that of another, resulting in a mantle of dominantly neutron matter (Ozawa *et al.,* 2001).

1.2 STATEMENT OF THE PROBLEM

The calculation of nuclear reaction cross sections is of crucial importance in revealing the structure of unstable nucleus. Both theoretical and the experimental techniques have been used with varying degrees of successes. Intensive experimental and theoritical results indicate that information about nucleus can be obtained at different energy level (i.e

low, intermediate and high energy collision). The large number of models had been applied for the calculation of nuclear reaction observables which gives an information about the unstable nuclei particularly halo. In this work, a computer program known as CSC GM Code will be used to numerically compute the one-nucleon removal cross section which is one of the observable for the core plus valence nucleon reaction system, with a view to investigate the halo nature of ^{11}Be, ^{13}C, ^{19}C and ^{37}Mg**.**

1.3 AIM AND OBJECTIVES

1.3.1 Aim

To numerically compute the one-nucleon removal cross section for the following reaction system,

$$^{11}\text{Be} + {}^{12}\text{C} \longrightarrow {}^{12}\text{C} + {}^{10}\text{Be} + \text{n} \quad \text{(i)}$$

$$^{13}\text{C} + {}^{12}\text{C} \longrightarrow {}^{12}\text{C} + {}^{12}\text{C} + \text{n} \quad \text{(ii)}$$

$$^{19}\text{C} + {}^{12}\text{C} \longrightarrow {}^{12}\text{C} + {}^{18}\text{C} + \text{n} \quad \text{(iii)}$$

$$^{37}\text{Mg} + {}^{12}\text{C} \longrightarrow {}^{12}\text{C} + {}^{36}\text{Mg} + \text{n} \quad \text{(iv)}$$

1.3.2 Objectives

1. To study the structure of the unstable nuclei in the reaction systems above for halo and skin.

2. To use CSC_GM code and calculate the total reaction cross section and one-nucleon removal cross section for ^{11}Be + ^{12}C, ^{13}C + ^{12}C ^{19}C + ^{12}C ^{37}Mg + ^{12}C reaction system.

3. To compare the computed result with experimental data with a view to establish the agreement of the Glauber model or otherwise.
4. To have a better understanding of internal structure of atomic nucleus.

1.4.0 SCOPE AND LIMITATIONS

1.4.1 Scope

This work involves the running of CSC_GM code several times for ^{11}Be, ^{13}C, ^{19}C and ^{37}Mg projectiles at different energies and analyzing the results.

1.4.2 Limitations

This computer code calculates the cross sections of various reactions for a core plus one valence-nucleon system in the framework of the Glauber model. The projectile nucleus is assumed to be a core plus one valence nucleon system, in which the valence nucleon is described with a pure configuration. The scattering amplitude is formulated in the Glauber theory. The phase-shift function between the core and the target and between the valence nucleon and the target are calculated in the optical-limit approximation, the integration over the valence-nucleon coordinates is performed by Monte Carlo integration, while the integration over the impact parameter is done with a trapezoidal rule as given in the code.

CHAPTER TWO (LITERATURE REVIEW)

2.1 INTRODUCTION

In recent years there has been much interest in the description of halo nuclei. These are weakly bound and spatially extended nuclear systems, so that some fragments of the nucleus (generally neutrons) have a high probability of being at distances larger than the typical nuclear radii. Different sophisticated models have been developed to describe the properties of halo nuclei, by calculating their reaction observables (such as reaction cross section, one-nucleon removal cross section etc). These include the Glauber model, which has been applied by many authors to determine these observables over a wide range of energies. The model gives the nucleus–nucleus interaction in terms of interaction between the constituent nucleons with a given density distribution. The model is a semi-classical one picturing the nuclear collision in the impact parameter representation and thus works well at high energy. This section discusses the theoretical background of the Glauber theory and how the problem of core plus one-nucleon removal was formulated.

2.2 GLAUBER MODEL

Developed by Roy Glauber (Nobel Prize in Physics, 2005) to address the problem of high energy scattering with composite particles. The Glauber model was first applied to nuclear scattering in the late 1950s. It forms the basis for the reaction cross section expression that was used to analyse the early interaction cross section measurements which confirmed the large halo size. Later, a few-body generalisation of the Glauber model was used to provide a more accurate prediction for this size, and provided the first

realistic calculation, which included the important few-body structure information of the halo and elastic scattering angular distributions for a number of nuclei.

A far more efficient approach for dealing with an *n*-body projectile is to use the few-body Glauber (FBG) model, which is based on the eikonal approximation. The eikonal approximation was introduced in quantum scattering theory by Moliere (Al-khalili, 2004) and later developed by Glauber who applied it to nuclear scattering, where he formulated a many-body, multiple scattering generalization of the method (Glauber 1985). In common with other semi-classical approaches, the eikonal method is useful when the wavelength of the incident particle is short compared to the distance over which the potential varies appreciably. This short wavelength condition is expressed in terms of the incident centre of mass wave number, $K_{0,}$ and the range of the interaction, R_0, such that

$$K_0 R_0 \gg 1. \qquad (2.0)$$

However, unlike short wavelength methods such as the WKB approximation, the eikonal approximation also requires high scattering energies, such that

$$E \gg |V_0|, \qquad (2.1)$$

where V_0 is a measure of the strength of the potential. In practice, and when V is complex, this high-energy condition is not critical and the eikonal approximation works well even when $E \approx |V_0|$ provided the first condition, Equation (2.0), holds and the model restricted to forward angle scattering. In that sense, the eikonal approximation covers both the Born and WKB limits and contains elements of both. The Glauber scattering amplitude can be derived starting from either the Schrödinger equation or the Lippmann-Schwinger equation.

2.2.1 Glauber's Derivation of the Scattering Amplitude

The time independent Schrodinger equation,

$$\left(\frac{-\hbar^2}{2m}\nabla^2 + V(\vec{r}) - \mathrm{E}\right)\Psi(\vec{r}) = 0, \tag{2.2}$$

where $\Psi(\vec{r})$ is the scattering wave function, which has a solution of the form

$$\Psi(\vec{r}) = Ae^{iS}, \tag{2.3}$$

where both $A(\vec{r})$ and $S(\vec{r})$ are purely real.

Now equation (2.2) may be written as

$$[\nabla^2 + k^2 - U(\vec{r})]\Psi(\vec{r}) = 0, \tag{2.4}$$

with $k^2 = \frac{2mE}{\hbar^2}$, (2.5a)

and $U(\vec{r}) = \frac{2m}{\hbar^2}V(\vec{r})$. (2.5b)

were $U(\vec{r})$ is called the reduced potential.

The Lippmann-Schwinger Equation:

The Schrodinger equation, (2.4) can be rewritten as

$$[\nabla^2 + k^2]\Psi(\vec{r}) = U(\vec{r})\Psi(\vec{r}), \tag{2.6}$$

where the right hand side is considered as inhomogeneous term. The general solution to this equation is written as

$$\Psi(\vec{r}) = \phi(\vec{r}) + \int \mathrm{G}(\vec{r}, \overrightarrow{r'})U(\overrightarrow{r'})\,\Psi(\overrightarrow{r'})\mathrm{d}\overrightarrow{r'} \tag{2.7}$$

where $\phi(\vec{r})$ is the solution of the homogeneous equation,

$$[\nabla^2 + k^2]\phi(\vec{r}) = 0, \tag{2.8}$$

and $G(\vec{r}, \vec{r'})$, is defined as (Riley et al., 2006)

$$[\nabla^2 + k^2]G(\vec{r}, \vec{r'}) = \delta(\vec{r} - \vec{r'}), \tag{2.9}$$

is the Green's function corresponding to the operator $[\nabla^2 + k^2]$.

In scattering problem the function $\phi(\vec{r})$ is simply the incident plane wave.

Therefore

$$\phi(\vec{r}) = e^{ik(\vec{n_i}.\vec{r})}. \tag{2.10}$$

The Green's function corresponding to the operator $[\nabla^2 + k^2]$ is given by (Afken 1985) as

$$G(\vec{r},\vec{r}) = -\frac{1}{4\pi}\frac{1}{|\vec{r} - \vec{r'}|}e^{ik|\vec{r} - \vec{r'}|}. \tag{2.11}$$

Now substituting equation (2.10) and (2.11) equation (2.7) becomes

$$\Psi(\vec{r}) = e^{ik(\vec{n_i}.\vec{r})} - \frac{1}{4\pi}\int \frac{1}{|\vec{r} - \vec{r'}|}e^{ik|\vec{r} - \vec{r'}|}\, U(\vec{r'})\Psi(\vec{r'})d\vec{r'}. \tag{2.12}$$

Substituting equation (2.5b), equation (2.12) is finally written as

$$\Psi(\vec{r}) = e^{ik(\vec{n_i}.\vec{r})} - \frac{1}{4\pi}\frac{2m}{\hbar^2}\int \frac{1}{|\vec{r} - \vec{r'}|}e^{ik|\vec{r} - \vec{r'}|}\, V(\vec{r'})\Psi(\vec{r'})d\vec{r'}. \tag{2.13}$$

This is Lippmann-Schwinger equation for scattering wave function $\Psi(\vec{r})$.

Now considering the relation for $f\left(\overrightarrow{n_\iota} - \overrightarrow{n_f}\right)$, the amplitude for scattering from initial $\overrightarrow{n_\iota}$ to the final direction $\overrightarrow{n_f}$, is given as

$$\lim_{\left(\overrightarrow{n_\iota} - \overrightarrow{n_f}\right)} \left[\Psi(\vec{r}) - e^{ik\left(\overrightarrow{n_\iota}.\overrightarrow{r}\right)}\right] = f\left(\overrightarrow{n_\iota} - \overrightarrow{n_f}\right)\frac{e^{ikr}}{r}, \tag{2.14}$$

Equation (2.13) yields

$$f\left(\overrightarrow{n_\iota} - \overrightarrow{n_f}\right) = \frac{1}{4\pi}.\frac{2m}{\hbar^2}T_{if}\ , \tag{2.15}$$

where

$$T_{if} = \int e^{\left(-ik\vec{n}_f\right)}\,\mathrm{V}\left(\vec{r}\right)\Psi(\vec{r})\mathrm{d}\vec{r}. \tag{2.16}$$

is called the transition matrix (T-matrix) or the transition operator.

Now the Glauber derivation proceeds as follows. Factoring the free incident plane wave, the scattering can be written as

$$\Psi(\vec{r}) = e^{ik\,\overrightarrow{n_\iota}.\vec{r}}F(\overrightarrow{r}), \tag{2.17}$$

Substituting equation (2.17) and letting $\vec{r}' = \overrightarrow{r} - \vec{r}''$, equation (2.13) becomes

$$F(\overrightarrow{r}) = 1 - \frac{1}{4\pi}.\frac{2m}{\hbar^2}\int \frac{e^{ik\vec{r}''}}{\vec{r}''}e^{-ik\,\overrightarrow{n_\iota}.\vec{r}''}\,\mathrm{V}\left(\overrightarrow{r} - \vec{r}''\right)\mathrm{F}\left(\overrightarrow{r} - \vec{r}''\right)\mathrm{d}\vec{r}''. \tag{2.18}$$

where

$$|\overrightarrow{r} - \vec{r}'| = \left|\overrightarrow{r} - (\overrightarrow{r} - \vec{r}'')\right| = |\vec{r}''| = \vec{r}'' \ ,$$

The integral equation (2.18) is solved approximately by expanding the integrand in a power series about $\theta'' = 0$ for every $\vec{r}''$, where θ'' is the polar angle of r, in spherical coordinates. The solution is given by (Glauber 1969) as

$$F(\vec{r}) = 1 - \frac{m}{ik\hbar^2}\int_0^{\infty} \mathrm{V}\left(\vec{r} - \vec{r}''\right)\mathrm{F}(\vec{r} - \vec{r}'')\mathrm{d}\vec{r}''. \tag{2.19}$$

This equation is written in Cartesian coordinate as

$$F(x,y,z) = 1 - \frac{i}{\hbar v}\int_{-\infty}^{z} V(x,y,z')F(x,y,z')dz', \tag{2.20}$$

where v is the initial velocity of the projectile.

This equation is solved as

$$F(r) = F(x,y,z) = e^{-\frac{i}{\hbar v}\int_{-\infty}^{z} V(x,y,z')dz'}. \tag{2.21}$$

Now substituting equation (2.21) into equation (2.17) immediately yield,

$$\Psi(\vec{r}) = A(\vec{r})e^{-\frac{i}{\hbar v}\int_{-\infty}^{z} V(x,y,z')dz'}, \tag{2.22}$$

where $A(\vec{r}) = e^{ik\,\vec{n_i}.\vec{r}}$, is the incident plane wavefunction of unit density in $\vec{r}$.

The result, equation (2.22) is the Glauber's approximation to the wavefunction.

Now substituting this equation back into (2.16) we obtain

$$T_{if} = \int e^{(-ik\,\vec{n_f}.\vec{r})}\mathrm{V}\left(\vec{r}\right)e^{ik(\vec{n_i}.\vec{r})}e^{-\frac{i}{\hbar v}\int_{-\infty}^{z} V(x,y,z')dz'}dr', \tag{2.23}$$

or $$T_{if} = \int e^{(i\vec{q}\,\vec{r})}\mathrm{V}(\vec{r}')e^{i\chi(\vec{r})}\mathrm{d}\vec{r}, \tag{2.24}$$

with

$$\chi(\vec{r}) = -\frac{i}{\hbar v}\int_{-\infty}^{z} V(x,y.z)dz', \tag{2.25a}$$

and $\vec{q} = k\left(\overrightarrow{n_i} - \overrightarrow{n_f}\right) = \overrightarrow{k_i} - \overrightarrow{k_f}$. (2.25b)

Equation (2.25b) represents the momentum transfer to the target from the impinging particle in unit of ħ. It is earlier argued that equation (2.22) is valid only for small angle scattering. We may neglect the component of $\vec{q}$ parallel to $\overrightarrow{n_i}$ i.e we may assume that $\vec{q}$ is perpendicular to the z-direction. With this further assumption, we have:

$$\vec{q}.\vec{r} \equiv \vec{q}.(x,y,z) = \vec{q}.(x,y) = \vec{q}.\vec{b}, \tag{2.25c}$$

With $\vec{b} \equiv (x,y)$,

and

$$\mathrm{d}\vec{r} = d^2\vec{b}dz,$$

Equation (2.24) then reduced to

$$T_{if} = \int d^2\vec{b}dze^{(i\vec{q}.\vec{b})}\,\mathrm{V}\left(\overrightarrow{b},\mathrm{z}\right)e^{\left(-\frac{i}{\hbar v}\int_{-\infty}^{z} V(x,y,z')dz'\right)}. \tag{2.26}$$

The vector $\vec{b}$ is actually the two-dimensional impact parameter vector perpendicular to z. In the approximate form of equation (2.26), however

$$T_{if} = -\frac{\hbar v}{i}\int d^2\vec{b}e^{(i\vec{q}.\vec{b})}\int_{-\infty}^{\infty} dz\frac{d}{dz'}e^{\left(-\frac{i}{\hbar v}\int_{-\infty}^{z} V(x,y.z)dz'\right)}. \tag{2.27}$$

substituting equation (2.27), equation (2.15) becomes

$$f(\overrightarrow{n_i} - \overrightarrow{n_f}) = \frac{ik}{2\pi}\int d^2\vec{b}e^{(i\vec{q}.\vec{b})}\left[1 - e^{(-\frac{i}{\hbar v}\int_{-\infty}^{z} V(x,y.z)dz)}\right]. \quad (2.28a)$$

This is the Glauber formula for potential scattering amplitude.

At low energy the factor $e^{(-\frac{i}{\hbar v}\int_{-\infty}^{z} V(x,y.z)dz)}$ approaches zero, therefore equation (2.28a) reduce to

$$f(\overrightarrow{n_i} - \overrightarrow{n_f}) = \frac{ik}{2\pi}\int d^2\vec{b}e^{(i\vec{q}.\vec{b})}. \quad (2.28b)$$

Which is simply the Born approximation to the scattering amplitude.

It has been assumed earlier that equation (2.28a) is valid only for small scattering angle θ. It has been shown that the validity criteria of equation (2.28a) (Gerjuoy and Thomas 1973) are

$$\theta < \frac{1}{(K\alpha)^{1/2}} \text{ when } \frac{V_0 a}{\hbar v} < 1, \quad (2.29a)$$

$$\theta \leq \left(\frac{V_0}{\hbar v K}\right)^{1/2} = \left(\frac{V_0}{2E}\right)^{1/2}, \text{ when } \frac{V_0 a}{\hbar v} > 1, \quad (2.29b)$$

where K is the initial wave number of projectile, v is the initial projectile velocity and α is the range of $V(\vec{r})$ i.e α is the distance (from the origin) within which $|V(\vec{r})|$ is of the order of its maximum magnitude V_0.

2.2.1.1 Derivation from Eikonal Approximations:

An alternative derivation of Eq. (2.28a), formula for the potential scattering amplitude, which starts directly from the eikonal approximation to the Schrodinger equation (2.3), thereby making it completely evident that the Glauber's formula is a

particular case of a whole class of possible eikonal approximations for the scattering amplitude runs as follows (Gerjuoy and Thomas1974):

Using the identity,

$$\nabla^2(AB) = \nabla\cdot\nabla(AB) = A\nabla^2 B + B\nabla^2 A + 2(\nabla A)\cdot(\nabla B).$$

with $\Psi(\vec{r})$ given by Eqn. (2.3), we have.

$$\nabla^2\Psi(\vec{r}) = [\nabla^2 A - A(\nabla S)^2 + 2i\nabla A \cdot \nabla S + iA\nabla^2 S]e^{iS}. \tag{2.30}$$

After substituting equation (2.30) in equation (2.4) the real and imaginary parts of equation (2.4) yield respectively.

$$\nabla^2 A - A(\nabla S)^2 + (k^2 - U)A = 0, \tag{2.31a}$$

$$2\nabla A \cdot \nabla S + A\nabla^2 S = 0, \tag{2.31b}$$

Equation (2.31b) can be rewritten in the form

$$div(A^2\nabla S) = 0. \tag{2.32}$$

and merely the flux conservation, since

$$\Psi^*\nabla\Psi - \Psi\nabla\Psi^* = 2iA^2\nabla S. \tag{2.33}$$

To this point there have been no approximations. The fundamental eikonal approximation is the assumption.

$$\frac{\nabla^2 A}{A} \ll k^2, \tag{2.34}$$

This approximation reduces (2.31a) to

$$(\nabla S)^2 = k^2 - U, \tag{2.35}$$

having solution

$$S(\vec{r}) - S(\vec{a}) = \int_a^r d\vec{r} \cdot \vec{n}\,(k^2 - U)^{1/2}. \tag{2.36}$$

where $a(\vec{r})$ is some initial point on the ray path through $\vec{r}$ and where at each point $\vec{r}' = \overrightarrow{r_0}$ on the ray path the direction of $\vec{n}(\overrightarrow{r_0})$ is perpendicular to the surface of constant S through $\overrightarrow{r_0}$.

Now expanding the square root in equation (2.36) gives:

$$(k^2 - U)^{1/2} = k\left(1 - \frac{U}{k^2}\right)^{1/2} = k\left(1 - \frac{1}{2}\frac{U}{k^2} + \frac{1}{8}\frac{U}{k^4} - \frac{1}{16}\frac{U}{k^8} + \cdots\right), \tag{2.37a}$$

A more explicit high energy approximation to the eikonal $S(\vec{r})$ is obtained by approximating the square root by first two terms of the expansion, namely

$$(k^2 - U)^{1/2} = k\left(1 - \frac{1}{2}\frac{U}{k^2}\right). \tag{2.37b}$$

Then equation (2.36) becomes

$$S(\vec{r}) - S(\vec{a}) = \int_a^r d\vec{r} \cdot \vec{n}\,\left(1 - \frac{1}{2}\frac{U}{k^2}\right). \tag{2.38}$$

which is valid when

$$U(\vec{r}) \ll k^2, \tag{2.39a}$$

i.e when

$$V(\vec{r}) \ll E, \tag{2.39b}$$

Equation (2.37) is still supposed to be integrated along the actual ray path perpendicular to the surface of constant $S(\vec{r})$. However, if the curvature of the ray path can be neglected and the z-direction chosen to coincide with the constant ray direction $\vec{n}$, then the point $a(\vec{r})$ has components (x, y, a_z) and equation (2.38) is now written as

$$S(x,y,z) - S(x,y,a_z) = \int_{a_z}^{r} dz' \left(k - \frac{1}{2}\frac{U(x,y,z)}{k}\right). \tag{2.40}$$

using equation (2.5b) we can write

$$\frac{1}{2}\frac{U(x,y,z')}{k} = \frac{2m}{\hbar^2 k}V(x,y,z') = \frac{2}{\hbar v}V(x,y,z'), \tag{2.41}$$

where $v = \frac{\hbar k}{m}$ is the initial velocity.

The above assumption, namely, the neglect of the ray curvature amounts to small scattering angle approximation. Now substituting equation (2.41), equation (2.40) becomes

$$S(x,y,z) - S(x,y,a_z) = \int_{a_z}^{r} k dz' - \frac{1}{\hbar v}\int_{a_z}^{r} dz'\, V(x,y,z')$$

$$= k(z - a_z) - \frac{1}{\hbar v}\int_{a_z}^{r} dz'\, V(x,y,z'). \tag{2.42}$$

However in scattering problems the incident wavefronts are the plane and uniformly spaced. thus at points $a_z \to -\infty$ we can set

$$S(x,y,a_z) = k a_z,$$

Consequently in the scattering problems, with the approximations made, and with plane wave incident along the positive $z = \vec{n}_i$ direction, equation (2.42) becomes ($a_z \to -\infty$)

$$S(x,y,z) = kz - \frac{1}{\hbar v}\int_{a_z}^{r} dz'\, V(x,y,z') \tag{2.43}$$

Moreover, if all the ray paths are supposed to be essentially parallel to $\vec{n}_i$(z-axis) then the spreading of the rays can be ignored and the conservation of the flux implies A^2 is a constant. With this therefore, using the approximate form (2.43), with A assumed constant and Z-direction along $\vec{n}_i$, equation (2.3) yield:

$$\Psi(\vec{r}) = e^{ik\,\overrightarrow{n_i}.\vec{r}}\, e^{-\frac{i}{\hbar v}\int_{-\infty}^{z} V(x,y.z)dz'}. \tag{2.44}$$

This is just the Glauber's approximation to the scattering wavefunction obtained in Eq.(2.22). The derivation of the Glauber formula (2.28a) for the scattering amplitude $f\left(\overrightarrow{n_i} - \overrightarrow{n_f}\right)$ follows as in equations (2.22) to (2.28a).

It is seen that Glauber derivation given above, starting from the integral equation (2.14) for exact solution of the scattering wavefunction $\Psi(\vec{r})$, involves essentially the same short wavelength and high energy assumptions as in the derivation of equation (2.44) from the eikonal approximation. However, Glauber's derivation has the virtue of clarifying the reason that the approximation equation (2.44) for $\Psi(\vec{r})$ is quite wrong for large $\vec{r}$. The reason for estimating $f\left(\overrightarrow{n_i} - \overrightarrow{n_f}\right)$ from equation (2.44) and (2.22) is that equation (2.16) demands accurate knowledge of $\Psi(\vec{r})$ only at the point $\vec{r}$ in the range of the potential; correspondingly because the Born approximation estimate of T_{if} employs $\Psi(\vec{r}) = e^{ik\,\overrightarrow{n_i}.\vec{r}}$ which presumably is not the best estimate of $\Psi(\vec{r})$ than equation (2.44) at values of $\vec{r}$ in the range of potential. The Glauber estimate should be an improvement on Born approximation whenever the conditions of (2.28a) are satisfied.

2.3 EXTENSION TO WIDER SCATTERING ANGLE:

At high incident velocities the criterion, equation (2.29a), limits the validity of equation (2.28a) for the scattering amplitude to quite small angles, often smaller than some scattering angles of experimental or even theoretical interest. At low incident velocities, where the criterion of equation (2.29b) applies, the angular range of validity of equation (2.28a) still should be small, because the approximation formula (2.38) underlying equation (2.28a) is valid only when equation (2.39) holds.

In view of this it is necessary to consider the possibility of extending equation (2.28a) for the Glauber scattering amplitude to wider scattering angles outside the validity range of equations (2.38) and (2.39). The eikonal approximation derivation has the virtue of immediately suggesting reasonable alternatives to equation (2.28a), possibly applicable to circumstances where equation (2.28a) is not valid. In particular when E is not very much greater than V (equation (2.39) is violated), the square root form of equation (2.36) can be retained instead of making the expansion in equation (2.37a). Also especially for scattering into wide angles not obeying equation (2.29) one can try to integrate along the actual ray path instead of assuming, as in equation (2.44), the integration path is perpendicular to $\vec{n}_i$.

Equation (2.28a) for Glauber scattering amplitude can be extended to wider scattering angles without any loss of simplicity and calculation convenience by choosing the integration path in equation (2.28a) along the straight line parallel to $\overrightarrow{n_\iota} - \overrightarrow{n_f}$ from $-\infty \; to \; \infty$. This extension of equation (2.28a) in which it becomes explicit to that for any $\overrightarrow{n_f}$ the direction of $\vec{b}$ is perpendicular to the z-direction lying along $f\left(\overrightarrow{n_\iota} - \overrightarrow{n_f}\right)$ in

potential scattering for arbitrary scattering angle $\cos^{-1}(\overrightarrow{n_i}.\overrightarrow{n_f})$. Because $\vec{q}$, given by (2.54b) is perpendicular to $\overrightarrow{n_i} - \overrightarrow{n_f}$ (or the average momentum $\frac{1}{2}(k_i + k_f)$, choosing the z-direction along in equation (2.25a) immediately yields equation (2.26) from equation (2.24) without any need to assume (as is previously assumed) that is perpendicular to the z-direction. Rather $\vec{q}$ is now automatically perpendicular to the z-direction, $e^{i\vec{q}.\vec{r}}$ now is precisely equal to $e^{i\vec{q}.\vec{b}}$and equation (2.28a), the scattering amplitude formula, then follows from equation (2.26) as before.

The Glauber's wide angle scattering formula (2.28a) with extension that the integration path is along the line parallel to $\overrightarrow{n_i} + \overrightarrow{n_f}$ from $-\infty\, to\, \infty$ has been quite successful at wide angles and, at intermediate and high energies.

The Glauber wide-angle scattering formula holds for Yukawa potentials or sums of Yukawa potentials (Gerjuoy and Thomas 1974). It also holds, at all energies for coulomb potential, which is the limit of the Yukawa potential $e^{-\mu r}/r$ as $\mu \to -\infty$. On the other hand the Glauber wide angle scattering formula is not successful for some potentials (eg. the Gaussian potential) even at very high energies. There still remains the problem of how to delineate the class of potentials $V(\vec{r})$ for which the Glauber wide angle potential scattering formula is valid in the high energy limit.

2.3.1 Theoretical Justification of the Wide Angle Formula

Since there are well-behaved potentials like the Gaussian potentials for which the Glauber's potential scattering formula appears to fail at wide angles in limit $K = (2mE)^{1/2}/\hbar$ (Byrd and Baetchy 2004), it is obvious that there is no wholly valid

justification for Glauber's wide angle formula. Nevertheless, the composite systems extension of the Glauber's wide angle formula (2.28a) has proved useful in atomic collision. However many different theoretical justifications to the Glauber wide angle scattering formula are available (Glauber 1969, Wallance 1973 etc) of which only the Glauber version will be presented here.

2.3.2 Glauber's Justification

For spherically symmetrical potentials,

$$V(x, y, z,) = V(r) = V\left[(z^2 + b^2)^{1/2}\right], \tag{2.45}$$

and the path integral over z' in equation (2.28a) depends only on the magnitude of $\vec{b}$.

Therefore introducing polar coordinates in the $\vec{b}$ plane, and remembering that the wide angle formula makes $\vec{q}$ parallel to $\vec{b}$ plane, equation (2.28a) reduces to (Glauber, 1985)

$$f\left(\overrightarrow{n_\iota} \rightarrow \overrightarrow{n_f}\right) = -ik \int_0^\infty db\, bJ_0\,(qb)\left[e^{2i\chi(b)} - 1\right], \tag{2.46a}$$

where J_0 is the Bessel function and

$$\chi(b) = -\frac{1}{\hbar v}\int_0^\infty dz V\left[(z^2 + b^2)^{1/2}\right], \tag{2.46b}$$

On the other hand, for the spherically symmetric potentials the exact scattering amplitude $f\left(\overrightarrow{n_\iota} \rightarrow \overrightarrow{n_f}\right)$ defined by equation (2.14) is expanded (Schiff, 1955) as

$$f\left(\overrightarrow{n_\iota} \rightarrow \overrightarrow{n_f}\right) = f(\theta) = \frac{1}{2ik}\sum_{l=0}^{\infty}(2l + 1)\left[e^{2i\delta_l} - 1\right]P_l(\cos\theta). \tag{2.47}$$

where $P_l(\cos\theta)$ is the Legendre function and δ_l is the scattering phase shift. At high energies where a large number of partial waves $l \gg 1$ contribute to equation (2.28a), the sum in equation (2.47) is replaced by integral, i.e.

$$f(\theta) = \frac{1}{2ik}\int_0^\infty dl(2l+1)\left[e^{2i\delta_l} - 1\right]P_l(\cos\theta). \tag{2.48}$$

The partial wave parameter l corresponding to the angular momentum $l\hbar$ is associated with the classical impact parameter b via (Gerjouy and Thomas, 1974)

$$l\hbar = k\hbar b,$$

or equivalently, at high energies and large l by

$$l = kb - \frac{1}{2}.$$

Thus equation (2.48) is replaced by

$$f(\theta) = -ik\int_{(2k)^{-1}}^\infty db(2l+1)\left[e^{2i\hat{\chi}\,(b)} - 1\right]P_{kb-1/2}(\cos\theta), \tag{2.49a}$$

where

$$\hat{\chi}\,(b) \equiv \delta_{kb-1/2}\,,$$

(2.49b) At large k the lower limit in equation (2.49a) can be replaced by zero. Therefore comparing equation (2.49a) and (2.46a), equation (2.46a) is a reasonable estimate of equation (2.47), i.e. the Glauber formula (2.49) will yield a reasonable estimate of exact scattering amplitude (Gerjouy and Thomas 1974) provided;

$$\hat{\chi}\,(b) = \chi(b), \tag{2.50a}$$

and,

$$P_{kb-1/2}(\cos\theta) \approx J_0(2kb\ \sin\tfrac{1}{2}\theta). \tag{2.50b}$$

2.4 PROPERTIES OF THE GLAUBER FORMULA

Glauber's wide formula (2.49) has a number of generally desirable properties for all potentials, including ease of calculations, time reversibility, unitarity and its high energy limiting behaviour.

2.4.1 High Energy Limiting Behaviour

It has already been pointed out (section 2.3) that equation (2.24) reduces to equation (2.28a) without further approximation when the z-direction is taken along$(\vec{n}_i + \vec{n}_f)$. However equation (2.24) differs from the Born approximation estimate to T_{if} only by the factor $e^{i\chi(b)}$ in the integrand. Therefore in the high energy limit $\upsilon \to \infty$, where $e^{i\chi(b)} \to 1$, the Glauber formula (2.28a) for $f(\overrightarrow{n_i} \to \overrightarrow{n_f})$ must reduce to Born approximation. This conclusion can be directly verify by expanding equation (2.28a) for $f(\overrightarrow{n_i} \to \overrightarrow{n_f})$ in decreasing powers of υ in which the leading term yields (Gerjouy and Thomas 1974)

$$T_{if} = \int d^2b e^{(i\,\vec{q}\,\cdot\vec{b})} \int_{-\infty}^{\infty} dz'\, V(x', y', z'). \tag{2.51}$$

where $\vec{b} = (x', y')$ is the two dimensional projectile of $\vec{r} = (x', y', z')$ onto the plane perpendicular to $\vec{n}_i + \vec{n}_f$ i.e onto the plane parallel to $\vec{q}$. This is to say, in equation (2.51) $\vec{q}.\vec{r} = \vec{q}\cdot\vec{b}$ without approximation. Therefore, written equation (2.51) condenses to the Born approximation,

$$T_{if} = \int d^2b e^{(i\,\vec{q}\cdot\vec{r})} V(\vec{r}). \tag{2.52}$$

without approximation.

For spherically symmetric potentials, term-by-term comparison of the Born series for $f(\overrightarrow{n_i} \rightarrow \overrightarrow{n_f})$ (obtained from equation (2.15) and (2.16) by integrating equation (2.13) in the powers series of the path integral over V, obtained by expanding in a power series of the term $e^{2i\chi(b)}$ in equation (2.46a)) has been made (Khayrallah 1976). This comparison sheds light on accuracy of Glauber's formula on the high energy limit.

2.5 DENSITY DISTRIBUTION OF NUCLEUS

2.5.1 Density Distribution of Stable Nuclei

The density distributions for stable nuclei, mainly charge distributions, have been well studied by electron scattering, isotope-shift measurements and studies of muonic atoms (Ozawa *et al.,* 2001). Good fits of the experimental data can be obtained by assuming a distribution of the form

$$\rho(r) = \rho_0 \left[1 + exp\frac{r-R}{a}\right]^{-1}, \tag{2.53}$$

The electron scattering and muonic atoms data are consistent with the parameters $\rho_0 = 0.17$ nucleon fm^{-3}, a = 0.54 fm and $R = 1.1A^{1/3}$ fm for all stable nuclei with mass number greater than 16 (Tanihata *et al.,* 2013). On the other hand, for light stable nuclei ($A \prec 20$), a harmonic-oscillator (HO)-type density distribution is sufficient to describe the experimental data. The HO-type density distributions including the contributions up to the *sd*-shell are given by the following equations (Ozawa *et al.,* 2001):

for $2 < Z < 8, 2 < N < 8$:

$$\rho_n(r) = 2\pi^{-3/2}\lambda^{-3}\left(1-\frac{1}{A}\right)^{-3/2} exp(-x^2)\left(1+\frac{N-2}{3x^2}\right), \quad (2.54)$$

$$\rho_p(r) = 2\pi^{-3/2}\lambda^{-3}\left(1-\frac{1}{A}\right)^{-3/2} exp(-x^2)\left(1+\frac{Z-2}{3x^2}\right), \quad (2.55)$$

for $Z < 8,\ N < 8$:

$$\rho_n(r) = 4\pi^{-3/2}\lambda^{-3}\left(1-\frac{1}{A}\right)^{-3/2} \frac{N}{N+8} exp(-x^2)\left(1+2x^2\frac{N-2}{15x^4}\right), \quad (2.56)$$

$$\rho_p(r) = 4\pi^{-3/2}\lambda^{-3}\left(1-\frac{1}{A}\right)^{-3/2} \frac{Z}{Z+8} exp(-x^2)\left(1+2x^2\frac{Z-2}{15x^4}\right). \quad (2.57)$$

where A, N and *Z* are the mass, neutron, and proton numbers, $x^2 = (r/\lambda)^2$ and λ denotes the size parameter.

The shapes for protons and neutrons are quite similar for stable nuclei. The differences in the proton and neutron distributions have been studied in detail for stable nuclei including ^{48}Ca and ^{208}Pb, which have many more neutrons than protons. However, no large differences in the radii between the proton and neutron distributions have been observed in stable nuclei (Tanihata 1996).

2.5.2 Density Distributions of Unstable Nuclei

The density distributions for unstable nuclei are quite different from those for stable nuclei. A significant character is the existence of skins and halos (Ozawa *et al.,* 2001). Although no large difference in the radii between the proton and neutron distributions has been observed in stable nuclei, most of the mean-field nuclear models predict a large difference in the radii for neutron (or proton) rich nuclei. Such neutron skins have been

observed in neutron-rich He isotopes (Tanihata 1995). In nuclei near the drip line, the separation energy of the last nucleon(s) becomes extremely small. The density distribution in such a loosely bound nucleus shows an extremely long tail, called a halo. Although the density of a halo is very low, it strongly affects the reaction cross sections, and leads to new properties for the nuclei.

2.5.3 Radioactive Ion Beam (RIB)

Since the middle of the 1980's, high-energy beams of secondary radioactive nuclei have been used for reaction studies with short-lived nuclei. The first measurement was to determine the interaction cross sections of the reaction between unstable nuclei and stable target nuclei. The Berkeley experiments carried out by Tanihata and his group involve the measurement of the interaction cross sections of helium and lithium isotopes and were found, for the cases of ^{6}He and ^{11}Li, to be much larger than expected. These corresponded to larger rms matter radii than would be predicted by the normal $A^{1/3}$ dependence (Bertsch, 1995) where A is the mass number of nucleus. Hansen and Jonson (Fulmante and Umashankar, 2013) proposed that the large size of these nuclei is due to the halo effect. They explained the large matter radius of ^{11}Li by treating it as a binary system of ^{9}Li core plus a dineutron (which implies that the two neutrons are stuck together and of course the n-n system is unbound) and showed how the weak binding between this pair of clusters could form an extended halo density.

Then, measurements were extended to the fragmentation cross sections and momentum distributions of fragments from radioactive projectiles. New-generation facilities of radioactive nuclear beams had provided a wide range of radioactive beams, and various

measurements have been made. Taking advantage of the high-intensity secondaries, elastic scatterings, inelastic scatterings, Coulomb excitations, and transfer reactions are now being studied.

2.5.4 Fragmentation

Measurements of the momentum distributions of fragments from the break-up of RI beams are good tools to search for some signature of a halo nucleus (Tanihata 1996). Also, the momentum distribution of the fragments provides in the first order the internal momentum distribution of removed nucleons, and thus provides means to study the wave function or density distribution of the valence nucleons. The fragmentation of unstable nuclei has been extensively measured at RI beam facilities for various nuclei (^{6}He to ^{26}P) over a wide range of energies (30 to 1000MeV) after the pioneering work of Tanihata and his group at Lawrence Berkeley Laboratory Bevalac in mid-1980's. In general, narrow momentum distributions of fragments correspond to a relatively large spatial extent of the valence nucleon(s). However, the break-up process seems not to be understood by a simple description. For example, the momentum distributions of ^{18}C from ^{19}C break-up have been measured at 30MeV and 1GeV (Ozawa et al., 2001). The two data sets do not show good consistency, although the data for ^{16}C from ^{17}C break-up shows a good agreement between the two energies.

Measurements of the nucleon(s) removal cross sections (σ_{-x}) give additional information concerning the size of valence nucleon(s). Two- and four-neutron removal cross sections have been used to estimate the difference in the proton and neutron density distributions in ^{6}He and ^{8}He (Ozawa *et al.,* 2001). Also, a combined analysis of (σ_{-x}) and (σ_{I}) is used

for identifying the "core plus valence nucleon" structure of a nucleus. Interaction cross section and the momentum distributions of fragments can be analyzed by the Glauber-model analysis with a core plus neutron(s) structure.

However, for example, in ^{19}C, a comparative analysis of both these experimental data fails to yield a consistent conclusion regarding a possible ground-state configuration. It was also suggested that a considerable change in the core of ^{19}C from a bare ^{18}C nucleus might take place.

2.5.5 Reaction Cross-Section (σ_R) Measurements

The reaction cross sections (σ_R) have been measured extensively for stable nuclei (proton to Ca) with various targets (proton to Pb) and for various energies (10 to 1000 MeV) (Ozawa *et al.,* 2001). The development of Radioactive Ion Beam (RI-beam) technology for intermediate energies ($\prec$ 100 MeV) allows one to measure σ_R for unstable nuclei.

Measurements of σ_R started at GANIL in the late 80s. And now, almost all RI-beam facilities, have programs for the measuring of σ_R for unstable nuclei: There are two major methods to measure σ_R at intermediate energies: (a) the associated γ-ray detection method (b) transmission method.

(a) In γ -ray detection, nuclear reaction is associated with the emission of at least one γ – ray. For example, an "ideal" γ -detector with 100% detection efficiency, it is necessary only to count the number of γ -events normalized to the number of incident particles and to the thickness of the reaction target. However, two uncertainties exist in this method. One is the efficiency of γ –ray detection; the other is the validity of the basic assumption, the emission of γ -rays in all reaction events. The second uncertainty is particularly large

for the reaction of a nucleus near to the drip lines. Because the nucleus is bound only by an extremely small energy, the removal of nucleons may occur with very soft collisions, and thus a γ -ray may not be emitted at all. Therefore, σ_R of near drip-line nuclei measured by this method may not be used to determine the nuclear sizes. Instead, the difference in σ_R from the transmission method and the γ-ray method provides support for the existence of loosely bound halo neutrons.

(b) The transmission method allows a direct measurement of σ_R without any interpretation by a theoretical model. However, complete particle identification is necessary after the reaction target. Such identification can be done by change of energy measurements at intermediate energies (>100 MeV) for light nuclei (A<20). A difficulty in this measurement is to identify an inelastic scattering and a reaction of particle removal only from the target. (It has to be noted that σ_I is the sum of the particle removal cross section from the projectile. Therefore no experimental interpretation exists for the determination of σ_I.) These events have to be identified by the change of the energy and momentum of the projectile. It therefore becomes difficult as the beam energy increases.

2.6 GLAUBER MODEL ANALYSIS

The most-used model for σ_I and σ_R is the Glauber model. Let $\sigma_{\alpha\beta}$ be the cross section for the reaction (Tanihata 1995; 1996; Ogawa *et al.,* 2001)

$$\mathrm{P}(|\Psi_0\rangle) + \mathrm{T}(|-K, \Theta_0\rangle) \longrightarrow \mathrm{P}(|q,\ \Psi_\alpha\rangle) + \mathrm{T}\big(\big|-\mathrm{K}-\mathrm{q}, \Theta_\beta\ \rangle\big), \qquad (2.58)$$

The initial projectile (P) and the target (T) are in their ground states. The relative momentum is $-\hbar\boldsymbol{K}$ .The projectile is excited by the reaction and goes to the state specified by α with a momentum transfer of $-.h\boldsymbol{q}$. The target nucleus receives a momentum transfer of $\hbar\boldsymbol{q}$ and goes to state β. It is defined that $\alpha = 0$ and $\beta = 0$ stand

for the respective ground states. The σ_R is obtained by summing $\sigma_{\alpha\beta}$over the possible final states$(\alpha\beta)$, except for $\alpha\beta = 00$

$$\sigma_R = \sum_{\alpha\beta \neq 00} \sigma_{\alpha\beta} = \int d\boldsymbol{b}\ \{1 - |exp[i\chi_{PT}(\boldsymbol{b})]|^2\}. \tag{2.59}$$

$$exp[i\chi_{PT}] = \langle \Psi_0 \Theta_0 \left| \prod_{i\in P} \prod_{j\in T} \left(1 - \Gamma_{ij}\right) \right| \Psi_0 \Theta_0 \rangle. \tag{2.60}$$

Here, Γ_{ij} is the profile function for NN scattering and *i, j* indicates a proton or a neutron. The second term in the curly brackets of Eq. (2.59) can also be written as $exp[-2\mathrm{Im}\chi_{PT}(\boldsymbol{b})]$, and represents the survival probability (also called the transmission function) of both the projectile and the target after a collision with impact parameter $\boldsymbol{b}$. σ_I is such a probability that the projectile loses at least one nucleon after a collision with a target nucleus, and can thus be obtained by summing $\sigma_{\alpha\beta}$ over all possible states $(\alpha\beta)$ except for $\alpha = 0$:

$$\sigma_I = \sum_{\alpha\beta=00} \sigma_{\alpha\beta} = \int db \left[- \langle \Psi_0 \Theta_0 \left| \prod_{i\in P} \prod_{j\in T} \left(1 - \Gamma^*{}_{ij}\right) \right| \Psi_0 \rangle \langle \Psi_0 \left| \prod_{i\in P} \prod_{j\in T} \left(1 - \Gamma_{ij}\right) \right| \Psi_0 \Theta_0 \rangle \right]. \tag{2.61}$$

Using Eqn. (2.59) (Ogawa *et al.,* 2011) estimated the difference between σ_{I} and σ_R; it was found to be less than a few percent for a beam energy higher than several hundred MeV per nucleon. Therefore, at high energy, the calculation of $\sigma_R$is used even for σ_{I} in most of the cases. However, the difference is expected to be larger at energy lower than 100 MeV. Equation (2.59) can be rewritten in other form

$$\sigma_R = 2\pi \int_0^\infty [1 - T(b)]\, bdb, \tag{2.62}$$

where $T(b)$, the transmission for impact parameter, $\boldsymbol{b}$ and is defined as the probability that at an impact parameter b the projectile pass through the target without interacting and it is calculated in the overlap region between the projectile and target. The Glauber model is then reduced to a calculation of the transmission.

2.6.1 Glauber Model with Optical-Limit Approximation

One of the simplest approximations to calculate $T(b)$ is the optical limit. In this approximation, the profile function is replaced by the NN cross sections under the zero range limit. The σ_R can then be calculated from the nucleon density distribution and the total NN cross sections

$$T(b) = exp\left[-\sum_{i,j}\sigma_{ij}\int d\vec{s}\,\rho^{z}{}_{T_i}(s)\rho^{z}{}_{P_j}\left(\left|\bar{b}-\bar{s}\right|\right)d\bar{s}\right], \tag{2.63}$$

where $\rho^z(s)$ is a z-direction integrated nucleon-density distribution,

$$\rho_{ki}^{z}(s) = \int_{-\infty}^{\infty}\rho_{ki}\left(\sqrt{s+z^2}\right)dz. \tag{2.64}$$

The index k = P (projectile) or T (target) and σ_{ij} are the nucleon–nucleon total cross sections in which indices *i, j* are used to distinguish a proton and a neutron. The nucleon density distribution in the nucleus is written as $\rho_{ki}(r)$. Equation (2.64) was used by Karol (Tanihata 1995) for estimating σ_R of heavy-ion collisions, assuming surface-fitted Gaussian density distributions. It reproduces the cross sections of stable nuclei reasonably well. This model was tested more precisely using a known density distribution. There, the proton-density distributions determined by electron scattering were used and the neutron distributions were assumed to be the same as that of the protons, except for the overall normalization. It was shown that these equations (Eqns. (2.62)–(2.64)) reproduce the

observed cross sections at high energy for all reactions involving some stable nuclei. Therefore, this simple optical-limit calculation of the Glauber model has been proved to work well at high energies. The energy dependence of the cross sections has been studied by Kox (Tanihata 1996). In his first analysis, the energy dependence of the $^{12}C + ^{12}C$ reaction cross sections at low energy would be reproduced reasonably well if the Coulomb deflection would be taken into account. It is rather surprising to see Glauber model work so well at low energy where the assumption used to drive the Glauber model is not necessary fulfilled. This assumption is not accurate, because some strong constrain were not taken into account in calculating some integrated observables such as reaction cross section. The energy dependence of the cross section, in principle, provides information about the density distribution, particularly the distribution at the tail part of the density.

2.6.2 Glauber Model for a Few-Body System

The optical limit of the Glauber model has been widely used for deducing the nuclear matter radii from the interaction and reaction cross sections. However, Al-Khalili and Tostevin (Ogawa et al., 2001) have pointed out that it may not be a good approximation if one applies the model to a loosely bound system, such as a nucleus with a neutron halo. This was also pointed out by Ogawa and Yabana, in their calculation of ^{11}Li (Ogawa *et al.,* 2001). In this refined model, a halo nucleus is decomposed into a core part and a halo part. In such a model the wave function of a halo nucleus is written as

$$\Psi_0 = \phi_0 \Phi_0 \,, \tag{2.65}$$

where Φ_0 is the core nucleus and ϕ_0 is the halo neutron wave function in the ground state of a halo nucleus (Ψ_0). In this case the reaction cross section is written as

$$\sigma_{reac} = \int d\boldsymbol{b} \left\{ 1 - exp[-2\mathrm{Im}\chi_c T(\boldsymbol{b})] \times \left| \langle \varphi_0 \left| \sum_i exp\left[i\chi_{n_i} T(\boldsymbol{b} + \boldsymbol{s_i}) \right] \right| \varphi_0 \rangle \right|^2 \right\}. \quad (2.66)$$

where i denotes the neutron in the halo and $\chi_c T$ is a phase-shift function between the core nucleus and the target nucleus; $i\chi_{n_i} T$ is that between a neutron and the target nucleus. Because the core nucleus is usually well bound, this part is calculated by the optical limit. It is worth noting the method for testing the validity of the de-coupling of the core and the halo neutron. The same Glauber model predicts the relation between the neutron removal cross sections and the interaction cross sections, as follows:

$$\sigma_I(\Psi_0) - \sigma_I(\Phi_0) = \sum_x \sigma_{nx}. \quad (2.67)$$

where $\sigma_I(\Psi_0)$ is the interaction cross section of the halo nucleus and $\sigma_I(\Phi_0)$ is that of the core nucleus. The right-hand side of the equation is the sum of the neutron and neutron removal cross sections of the halo neutrons up to all halo neutrons. The index x denotes the number of removed neutrons.

Al-Khalili and Tostevin (Al-khalili 2004) applied this core plus halo method to ^{11}Li, ^{11}Be, and ^{8}B halo nuclei for the first time and found that this new model gives a smaller cross section than that obtained from the optical limit if one uses the same wave function. As a result, the deduced RMS matter radii of halo nuclei are 0.1 to 0.2 fm larger than that deduced from the optical limit. Therefore, this model is recently being commonly used to

deduce the radii of halo nuclei. The validity of this method for determining the matter distribution is considered to be better, theoretically, than the optical-limit calculation.

The main feature of the original Glauber calculations is the "optical limit", used to make the full multiple scattering integral numerically tractable. With the advent of desktop computers, the "Glauber Monte Carlo" (GMC) approach emerged as a natural framework for use by more realistic particle production codes (Miller *et al.,* 2007). The idea was to model the nucleus in the simplest way, as uncorrelated nucleons sampled from measured density distributions. Two nuclei could be arranged with a random impact parameter b and projected onto the x-y plane. Then interaction probabilities could be applied by using the relative distance between two nucleon centroids as a stand-in for the measured nucleon- nucleon inelastic cross section.

Different computer program codes had been developed to numerically calculate the physical observables present in the framework of Glauber model. This include,

The CSC_GM Code developed by (B. Abu-Ibrahim *et al.,* 2003*)* which is a *Fortran 90* program to calculate cross sections for various reactions between composite particles in the framework of Glauber theory. The projectile nucleus is described as a core plus one valence-nucleon system. The input data needed for the calculation are the core and target densities and the nucleon–nucleon profile function. The single-particle wave function of the valence nucleon may be provided by a user or generated by the code if appropriate quantum numbers of the wave function are specified. Multiple integrations involving the valence-nucleon wave function are performed by a Monte Carlo technique with Metropolis algorithm. The program gives the total reaction cross section, the one-nucleon removal cross section, the elastic differential cross section, and the longitudinal

momentum distribution of the core fragment. The description of this program is given in the next chapter.

2.4 REVIEW OF RELATED LITERATURE

Calculation of nuclear reaction cross-sections for stable and unstable projectiles and targets within Glauber model, using densities obtained from various relativistic mean field formalisms was done by (Abu-Ibrahim, *et al.,* 2002). They observed that the calculated reaction cross-sections are comparable with the experimental data in some specific cases. They also evaluated the differential scattering cross sections at several incident energies, and observed that the results found from various densities are similar at smaller scattering angles, whereas a systematic deviation is noticed at large angles. In general, their results agree fairly well with the experimental data.

(Abu-Ibrahim *et al.,* 2002) calculated the nucleus–nucleus cross sections using nucleon–nucleus optical potentials in the framework of Glauber theory. The reaction cross sections for various light nuclei including loosely bound nuclei were constructed from the nucleus–nucleus phase shift functions which need the nuclear density and the optical potential as an input. They also found that at high energy the calculated reaction cross sections are in agreement with experimental data within error bar. At lower energy, a correction beyond the eikonal approximation is needed.

The CSC_GM Code developed by (B. Abu-Ibrahim *et al.,* 2002*) which is also a Fortran 90 program* to calculate cross sections for various reactions between composite particles in the framework of Glauber theory. The projectile nucleus is described as a core plus one valence-nucleon system. The input data needed for the calculation are the core and target densities and the nucleon–nucleon profile function. The single-particle

wave function of the valence nucleon may be provided by a user or generated by the code if appropriate quantum numbers of the wave function are specified. Multiple integrations involving the valence-nucleon wave function are performed by a Monte Carlo technique with Metropolis algorithm. The program gives the total reaction cross section, the one-nucleon removal cross section, the elastic differential cross section, and the longitudinal momentum distribution of the core fragment. The code was first run on Unix operating system.

Single-neutron removal reactions from ^{15}C and ^{11}Be Deviations from the eikonal approximation had been carried out (Bazin *et al.,* 2002). The momentum distributions of the residual nuclei after one-neutron removal have been measured using the Continuum Discretized Coupled-Channels (CDCC method) in coincidence with gamma rays identifying the distributions associated with the excited and ground state levels of these residues.

A fortran-77 code title momdis was developed by (Bertulani and Gade, 2006) to calculate the momentum distributions in stripping and diffraction dissociation reactions. A Glauber model was used with the scattering wavefunctions calculated in the eikonal approximation. The program is appropriate for knockout reactions at intermediate energy collisions. It is particularly useful for reactions involving unstable nuclear beams, or exotic nuclei (e.g., neutron-rich nuclei), and studies of single-particle occupancy probabilities (spectroscopic factors) and other related physical observables. The program calculates bound wave functions, eikonal S-matrices, total cross-sections and momentum distributions of interest in nuclear knockout reactions at intermediate energies. The program solves the radial Schrödinger equation for bound states. The S-matrices were

obtained using eikonal wavefunctions and the eikonal phase-shifts. The momentum distributions were obtained by means of a Gaussian expansion of integrands. Main integrals are performed with the Simpson's method. Sample calculation include the computation of momentum distribution for $^{15}C + {}^{9}Be \rightarrow {}^{14}C + X$ at 103 MeV energy reaction system.

An investigation of high-energy one-neutron removal reactions on 23 neutron-rich p-sd shell nuclei has been presented by (Sauvan, 2003). They studied the isotopic chains extending from strongly bound near stable systems to weakly bound near dripline nuclei. They also explored the evolution of structure with isospin, as expressed by the core fragment observables (longitudinal and transverse momentum distributions and inclusive cross sections). They found that In terms of weakly bound nuclei, there is a need to employ realistic wavefunctions in the analysis of the reaction cross sections. Similar effects must almost certainly be addressed in the analysis of high energy, single nucleon removal

One-neutron removal cross sections from elastic and inelastic breakup contributions for some neutron rich isotopes had been calculated using the Relativistic Mean Field (RMF) theory by (Panda *et al.,* 2009). It was observed from their results somehow overestimate for lighter and underestimated for heavier nuclei. The origin of this discrepancy may be due to the spherical densities considered in the calculations.

Within the optical limit approximation of Glauber multiple scattering model (Eiden *et al.,* 2010) calculated the total reaction cross section for proton scattering on some stable and unstable nuclei. They described the densities of the target nuclei by both relativistic mean field (RMF) and field motivated effective Lagrangian (E-RMF)

approach. They found that the values of σ_R were strongly correlated to the values of slope parameter of nucleon-nucleon (NN) scattering amplitude. Introducing Coulomb correction provides results close to the experimental data at low energy. In general, the application of optical limit approximation succeeded in describing σ_R in the entire range of energy, with suitable values for slope parameter of NN scattering amplitude.

The study of ground state properties (binding energy and charge radius) using relativistic mean filed formalism (RMF) for Mg-isotopes and the calculation of total reaction cross section of $^{24-40}$Mg+^{12}C reactions at projectile energy 240 MeV, using Glauber model with the conjunction of densities from relativistic mean field formalism was done by (Sharma *et al.,* 2015). They found a remarkable agreement of estimated values of reaction cross sections with experimental data except for ^{37}Mg isotope. In view of this, they examined the halo status of ^{37}Mg through higher magnitude of rms radius and small value of longitudinal momentum distribution. They also determined the One-neutron removal cross section by calculating both the elastic and inelastic component. They also used a large diffuseness parameter (3.5 fm) in the calculations which is very large compared to 0.6 fm given by Wood-Saxon.

Evaluation of the scattering amplitude of the Glauber model without any ad hoc approximation using Monte Carlo integration was carried out by (Abu-Ibrahim *et al.,* 2013). The advantage of this approach is that one can use accurate, sophisticated wave functions of colliding nuclei. The approach has the strength that makes it possible to directly relate cross sections to relevant wave functions.

CHAPTER THREE

METHODOLOGY

3.0 INTRODUCTION

In order to be able to compare the results obtained from this program with the other approaches, few model inputs are needed. The important ones among them are the nuclear density profile of the colliding nuclei and the energy dependence of the nucleon-nucleon cross section. This chapter describes how the work was carried out, the input data to be read by the program and a brief description on how the program works are given. Brief explanations of the cross-section for the different reactions systems are also included.

3.1 THE CSC_GM CODE

The CSC_GM code (Cross Section Calculations in the Glauber Model), a Fortran 90 program that was originally run on *UNIX* operating system, was obtained from the CPC Program Library, Queen's University of Belfast, Northern Ireland, under catalogue identifier ADRC. The program is made up of three categories of files: physics source code, input files and output files. The physics source code is the main source code which contains the routine for the actual computations. The input files contain data to be read into the main program at run-time. The output files keep the results of the computation. First thing done was the successful installation of the program code (CSC_GM) in the computer. This requires familiarity with the computer's operating system. Secondly, the compilation of program code which was done using '*gnu compiler*' in the digital *Linux* operating system (Ubuntu 14.04). Third was the testing of the compiled program using the example enclosed in the code and it runs interactively with the result obtained found to be as expected. Lastly the compiled program was used in carrying out this work and

the data generated were saved in the output files which were later imported into the graphics software *Origin50* for plotting.

The quantities to be calculated in this study include the total reaction cross section, one-nucleon removal cross section and elastic and inelastic reaction cross section, of core plus valence-nucleon system, of the following reactions;

$^{11}Be + {}^{12}C \longrightarrow {}^{12}C + {}^{10}Be + n$ (i)

$^{13}C + {}^{12}C \longrightarrow {}^{12}C + {}^{12}C + n$ (ii)

$^{19}C + {}^{12}C \longrightarrow {}^{12}C + {}^{18}C + n$ (iii)

$^{37}Mg + {}^{12}C \longrightarrow {}^{12}C + {}^{36}Mg + n$ (iv)

3.2 PROGRAM DESCRIPTION

The preparation of the input files to be used by the main program is as follows

csc.inp: This input file defines a reaction system, a cross section to be calculated, target and core densities, and some control parameters.

wf.inp: The code generates the single-particle wave function from the parameters of this input file.

The radial part of the single-particle wave function, $R_{nlj}(r) = ru_{nlj}(r)$, which is used as the guiding function $w(\boldsymbol{x})$ is obtained by solving a Schrödinger equation,.

$$\frac{d^2R(r)}{dr^2} + \frac{2\mu}{\hbar^2}\left[E - U(r) - \frac{l(l+1)\hbar^2}{2\mu r^2}\right]R(r) = 0, \quad (3.1)$$

with a potential U (r)

$$U(r) = -V_0 f(r) + V_{ls}(l.s){r_0}^2 \frac{1}{r}\frac{d}{dr}f(r) + V_{coul}. \quad (3.2)$$

where $f(r) = \left[1 + \exp\frac{r-R}{a}\right]^{-1}$ with $R = r_0 A_C^{1/3}$.

where r_0 and a are the radius and diffuseness parameters in fm respectively. V_0 is the initial depth of the potential. $V_{ls} = 17$ MeV (Ogawa *et al.,* 2003). The depth of the potential V_0 is adjusted so as to fit the energy eigenvalue specified by the quantum numbers *nlj* to that requested by the user. The input file is read by the subroutine **wavefn** which calculates the radial part of the single-particle wave function.

The preparation of the data needed for the calculation is completed at this stage.

3.3 INPUT DATA

The input data specify the reaction system, the type of cross section, the target and core densities, and the control parameters of the Metropolis algorithm etc. The input data for the $^{13}C + ^{12}C$ reaction system are read from the file **csc.inp,** for example in Table 1. The first line gives the mass numbers of the target, projectile and core (A_T, A_P, and A_C), the second line gives the charge numbers of those nuclei (Z_T, Z_T, and Z_C). This code assumes, $A_P - A_C = 1$. The third line defines the incident energy of the projectile per nucleon (in MeV). The fourth line defines the parameters of the nucleon–nucleon profile function, σ_{NN} (in fm^2), α, and β (in fm^2). The fifth line gives the orbital angular momentum of the valence nucleon. The sixth line specifies the condition for the Monte Carlo quadrature, the number of configuration points (N_S), the step size (δ in fm) for the random walk in the Metropolis algorithm, and the seed number for generating random numbers (irand). The seventh line is the control parameter for the single-particle wave function of the valence nucleon. The ninth line gives the number of Gaussians used to fit the target and the core densities. The tenth lines give the coefficients c_i and the ranges a_i

of the Target density. The last line gives the coefficients c_i and the ranges a_i of the core density (in fm^{-2}).

Table1: The input data of $^{13}C + ^{12}C \longrightarrow ^{12}C + ^{11}C + n$ reaction system.

S/N	INPUT PARAMETERS	VALUES
1	Mass numbers of target, projectile and core: (A_T; A_P; A_C)	12, 13, 12
2	Atomic numbers of target, projectile and core: (Z_T; Z_P; Z_C)	6, 6, 6
3	Incident Energy per nucleon (in MeV)	900
4	Profile function parameters (σ_{NN}, α and β in fm^2)	4.17, -0.21, 0.200
5	l (angular momentum quantum number)	0
6	Monte Carlo parameters (Ns, δ, irand)	500000, 2.5, −11213
7	icond1 (1:available, 0: not available)	0
8	Number of Gaussians used to fit the core and target densities	2
9	Coefficient c_i, range a_i (in fm^{-2}) of the Target	-1.25421 0.39907 1.39728 0.355553
10	Coefficient c_i range a_i (in fm^{-2}) of the Core	-1.25421 0.39907 1.39728 0.355553

Table 2 wf.inp input file

S/N	INPUT PARAMETERS	VALUES
1	Initial depth V_0 of the optical potential (in MeV)	70.0
2	Diffuseness parameter (in fm) a	0.6
3	Radius parameter r_0 (in fm)	1.2
4	Energy eigenvalue for the valence nucleon (in MeV)	-4.946
5	j value for the valence nucleon orbit	0.5
6	Node number for the valence nucleon orbit	1

3.4 OUTPUT DATA

The results of the calculation are written on different output files according to the quantity of interest. For one-nucleon removal cross sections the results are written in the file **reac.out,** which contain the mass and charges of the projectile and target, energy of projection, projectile and core total reaction cross section and the contribution to both elastic and inelastic cross sections. The sample of the output is given in Table 3.

Table 3 the output of $^{13}C + ^{12}C$

S/no	Cross Section (in mb)	Result
1	Projectile reaction cross section	924.6
2	Core reaction cross section	894.6
3	Nucleon removal cross section	29.8
4	N-removal (elastic)	3.5

3.5 CROSS-SECTION FOR THE REACTION

Consider the reaction of a projectile nucleus P with a target nucleus T. At the initial stage of the reaction, the projectile is in the ground state described with an intrinsic wave function ψ_o impinges with momentum $\hbar k$ = (0, 0, $\hbar$K*)* on the target in its ground state described with an intrinsic wave function Θ_c. The center-of-mass wavefunction is removed from ψ_a (Θ_0). At the final stage of the reaction, the projectile goes to the state *a* specified by a wave function $\psi_a$and the target goes to the state *c* specified by a wave function Θ_c . The state *a* is not necessarily a bound state but may be a continuum state that includes some fragments. The momentum transferred from the target to the projectile is $\hbar \boldsymbol{q}$**,** (Tanihata, 1996; Ozawa *et al.,* 2001),.

The scattering amplitude for this reaction is written in the Glauber theory as an integral over the impact parameter $\boldsymbol{b}$ between the projectile and the target (Adamu, 2013; Abu-ibrahim *et al.,* 2002) as

$$F_{ac}(q) = \frac{\mathrm{i}k}{2\pi}\int d\boldsymbol{b}\mathrm{e}^{-\mathbf{q}.\mathbf{b}}\langle\psi_a\Theta_c\big|1-\prod_{i\in P}\prod_{j\in T}\big(1-\Gamma_{ij}\big)\big|\psi_{\mathrm{o}}\Theta_0\rangle, \tag{3.3}$$

The profile function Γ in Eq. (3.3) is used to fit empirical nucleon-nucleon scattering amplitudes and is taken as:

$$\Gamma(\boldsymbol{b}) = \frac{1-i\alpha}{4\Pi\beta}\sigma_{NN}e^{-b^2/2\beta}. \tag{3.4}$$

The parameters σ_{NN}, α and β usually depend on either the proton–proton (neutron–neutron) or proton–neutron case, but we assume that some appropriate average values taken from (El-Din and Hassan 2010, Sharma et al,. 2013) to be use in this calculations. The argument of Γ_{ij} in Eq. (3.4) is $\boldsymbol{b}+\boldsymbol{s}_i^P-\boldsymbol{s}_j^T$ which stands for the impact parameter between *ith* and *jth* nucleons. Here $\boldsymbol{s}_i^P(\boldsymbol{s}_i^T)$ is the two-dimensional coordinates comprising the *x*- and *y*-components of the *ith* nucleon coordinate in the projectile (target) relative to its center-of-mass coordinate. Here σ_{NN} is the total nuclear reaction cross section of NN collision, α is the ratio of the real to the imaginary part of the forward nucleon-nucleon scattering amplitude and β is the slope parameter. The slope parameter determines the fall of the angular distribution of the N-N elastic scattering.

The integrated cross section for this reaction is given by

$$\sigma_{ac} = \int\frac{dq}{\kappa^2}|F_{ac}(\boldsymbol{q})|^2\ . \tag{3.5}$$

3.5.1 Total Reaction Cross Section

The total reaction cross section is obtained by summing σ_{ac} over all possible final states *ac* except for the elastic Channel (Ogawa *et al.,* 2003) :and is given as

$$(P+T) = \sum_{ac \neq 00} \sigma_{ac}, \tag{3.6}$$

The projectile-target total cross section is given by

$$\sigma_{reac}(P+T) = \int db \left(1 - \left|e^{i\chi_{PT}(b)}\right|^2\right). \tag{3.7}$$

The projectile is assumed to be a system of a core nucleus coupled with a valence nucleon. Its ground-state wave function is given by equation (2.65)

In this code, however, the Optical Limit Approximation (OLA) was used for the integration involving the coordinates of the core and the target; while the integration for the valence nucleon coordinate was perform without any approximation (Abu-ibrahim *et al.,* 2002; Ogawa *et al.,* 2003). In this treatment, the phase-shift function χ_{PT} is given by

$$e^{i\chi_{PT}(\boldsymbol{b})} = \langle \varphi_0 \left| e^{i\chi_{CT}(\boldsymbol{b}_C) + i\chi_{NT}(\boldsymbol{b}_C + s)} \right| \varphi_0 \rangle. \tag{3.8}$$

with $\boldsymbol{b}_C = \boldsymbol{b} - \frac{1}{\mathrm{A_p}}\boldsymbol{s}$, $\mathrm{A_p}$ is the projectile mass number, χ_{CT} is the core-target phase-shift function, χ_{NT} is the nucleon-target phase-shift function and $\boldsymbol{s}$ is the two-dimensional coordinates comprising the *x*- and *y*-components

Also the core-target total reaction cross section is given by

$$\sigma_{reac}(C+T) = \int db \left(1 - \left|e^{i\chi_{CT(b)}}\right|^2\right). \tag{3.9}$$

3.5.2 One-Nucleon Removal Cross Section

The one-nucleon removal cross section σ_{-N} is separated into elastic and inelastic cases and is given by the sum of the two (Shukla *et al.,* 2014).

The cross section due to the elastic breakup process is given by

$$\sigma_{-N}^{el} = \int db \left\{ \langle \varphi_0 | e^{-2lm\chi_{CT}(b_C)-2lm\chi_{NT}(b_C+s)} | \varphi_0 \rangle - \left| \langle \varphi_0 | e^{i\chi_{CT}(b_C)+\chi_{NT}(b_C+s)} | \varphi_0 \rangle \right|^2 \right\}.$$

(3.10)

While the cross section from inelastic breakup is given by

$$\sigma_{-N}^{inel} = \int db \, \langle \varphi_0 | e^{-2lm\chi_{CT}(b_C)} - e^{-2lm\chi_{CT}(b_C-s)-2lm(b_C+s)} | \varphi_0 \rangle.$$

(3.11)

The one-nucleon removal cross section for halo nuclei is approximately equal to the difference between the two reaction cross sections,

$$\sigma_{reac}(P+T) - \sigma_{reac}(C+T). \tag{3.12}$$

The core-target phase-shift function, χ_{CT} and the nucleon-target phase-shift function, χ_{NT} are defined through the relevant densities of the target (ρ_T) and core (ρ_C) (Ogawa *et al.,* 2003) by

$$i\chi_{CT}(\boldsymbol{b}) = -\int \mathrm{d}\boldsymbol{r} \int \mathrm{d}r' \, \rho_C(\boldsymbol{r})\rho_T(\boldsymbol{r}')\Gamma(\boldsymbol{b}+\boldsymbol{s}-\boldsymbol{s}').$$

(3.13)

$$i\chi_{NT}(\boldsymbol{b}) = -\int \mathrm{d}\boldsymbol{r} \, \rho_T(\boldsymbol{r})\Gamma(\boldsymbol{b}-\boldsymbol{s}). \tag{3.14}$$

The density ρ is normalized to the mass number of a nucleus, $\int \mathrm{d}r \, \rho(\boldsymbol{r}) = \mathrm{A}$, and it is assumed to be given by a combination of Gaussians: (Shukla *et al.,* 2014, and Sharma *et al.,* 2013).

$$\rho(r) = \sum_i c_i \, \mathrm{e}^{-a_i r^2}. \tag{3.15}$$

where c_i is Gaussian coefficient to fit the nuclei density and a_i is the range.

3.6 PROGRAM SUBROUTINES

The program contains subroutine and function subprograms depending on the quantity to be computed.

3.6.1 Subroutine Const

This subroutine calculates the norm, rms. radius and constant of the single particle wave function.

3.6.2 Subroutine rcsn

This subroutine calculates the projectile-target total reaction cross section using $\sigma_{\mathrm{reac}}(\mathrm{P}+\mathrm{T})$, the core-target total reaction cross section $\sigma_{\mathrm{reac}}(\mathrm{C}+\mathrm{T})$, the one-nucleon removal cross section $\sigma_{-\mathrm{N}}$, and the contributions to $\sigma_{-\mathrm{N}}$ from the elastic and inelastic breakup processes, from equation (3.7), (3.9), (3.10), (3.11) and (3.12) respectively

3.6.3 Function uprd3

The multi-dimensional integration over the valence-nucleon coordinates, which are needed in the subprograms **rcsn**, were performed with the Monte Carlo technique. The guiding function w(**x**) in the random walk with Metropolis algorithm is chosen differently, depending on the type of integration. In the subroutines **rcns**, $w(\boldsymbol{x})$ was chosen to be the radial part of the single particle wave function and calculated in this function subprogram by using a linear interpolation from the data tabulated in wf.inp.

3.6.4 Subroutine gene

In this subroutine, using the subroutine **metro,** the set of configuration or integration point used to perform the multi-dimensional integration for all b values, were generated, using the random walk with the Metropolis algorithm according to a suitably chosen values of the guiding function.

3.6.5 Function zchnt

The nucleon-target scattering phase-shift function $i\chi_{NT}$ equation (3.14) in which the various reaction cross sections are constructed, from is calculated in this function subprogram.

3.6.6 Function zchct

In this function subprogram the core-target elastic scattering phase-shift function $i\chi_{CT}$ equation (3.13) in which the various reaction cross sections are constructed from is calculated.

3.6.7 Subroutine eng

The cross sections of nuclear reactions are always measured in the laboratory coordinate system where the target is at rest. But it is more fundamental and more convenient to analyze them relative to the centre of mass of the projectile and the target namely in the Centre of Mass (C.M) system. This subroutine transforms from Laboratory to C.M. frame.

3.6.8 Subroutine wavefn

This subroutine calculates a radial part of the single-particle wave function Eqn. (3.1) by adjusting the central potential depth so as to reproduce the binding energy. The potential types are: Woods-Saxon + Coulomb + spin-orbit.

CHAPTER FOUR

RESULTS AND DISCUSSION

4.1 THE REACTION SYSTEMS

4.1.1 $^{11}Be + {}^{12}C \longrightarrow {}^{10}Be + {}^{12}C + n$

The ^{11}Be nucleus is treated as a ^{10}Be + neutron system. The neutron is in the $1s_{1/2}$ orbit with $n = 1$, $l = 0$, $j = 0.5$ and the separation energy of $\varepsilon = 0.503$ MeV (Tanihata, 1996).The parameters of the profile function are taken from (Sharma, *et al.,* 2013; Panda *et al.,* 2013; Shukla *et al.,* 2014; El-din and Hassan, 2010).

4.1.2 $^{19}C + {}^{12}C \longrightarrow {}^{18}C + {}^{12}C + n$

The ground state of ^{19}C is assumed to be ^{18}C + neutron system. The valence neutron is in the $1s_{1/2}$ orbit with $n = 1$, $l = 0$, $j = 0.5$, and the separation energy $\varepsilon = 0.24$ MeV (Tanihata, 1996). The appropriate average values of the profile function parameters (Eq. 3.4) which depend on the isospin of the nucleons are taken from (Shukla *et al.,* 2014).

4.1.3 $^{37}M + {}^{12}C \longrightarrow {}^{36}M + {}^{12}C + n$

The ground state of ^{37}Mg is assumed to be ^{36}Mg + neutron system. The valence neutron is in the $2s_{1/2}$ orbit with $n = 2$, $l = 0$, $j = 0.5$, and the separation energy $\varepsilon = 0.22$ MeV (Shubhchintak *et al.,* 2015).

4.2 THE REACTION CROSS SECTIONS

4.2.1 Total Reaction Cross Section

The total reaction cross sections for ^{11}Be, ^{19}C and ^{37}Mg were calculated using the CSC_GM Code at different energies and the results were compared with the experiment as shown in the Tables 4.1, 4.2 and 4.3.

Table 4.1: comparison of the computed total reaction cross sections at high energy with the experiment. Experimental results for ^{11}Be and ^{19}C obtained from (Ozawa *et al.,* 2001) ^{37}Mg from (Sharma *et al.,* 2010).

Projectile	Energy (MeV)	CSC_GM Code (mb)	Experiment (mb)
^{11}Be	730	961	942 ±8
^{19}C	960	1215	1231 ±28
^{37}Mg	900	1494	1472±30

Table 4.2: Comparison of the computed total reaction cross sections at intermediate energy with the experiment. Experimental results for ^{11}Be and ^{19}C obtained from (Sharma *et al.,* 2013) and ^{37}Mg from (Sharma *et al.,* 2014).

Projectile	Energy (MeV)	CSC_GM Code (mb)	Experiment (mb)
^{11}Be	100	1198	993
^{37} Mg	240	1373	1536±15
^{19}C	100	1451	1562

Table 4.3: Comparison of the computed total reaction cross sections at low energy with the experiment. Experimental results for ^{11}Be and ^{19}C obtained from (Ozawa *et al.,* 2001) and ^{37}Mg from (Sharma *et al.,* 2014).

Projectile	Energy (MeV)	CSC_GM Code (mb)	Experiment (mb)
^{11}Be	30	1715	1560 ± 30
^{37}Mg	49	1703	1601 ± 130

4.2.2 One-Nucleon Removal Cross Section

The energy dependence of the one-nucleon removal cross section for these nuclei were studied. Parameters for the input files **csc.inp** which determine the quantity to be calculated and **wf.inp**, that will be read by the subroutine **wavefn** to calculate the radial part of the single-particle wave function were also given. Note that the one-nucleon removal cross section is given by the sum of elastic and inelastic part as discussed in Section 3.5.

4.2.2.1 Neutron-Removal Cross Section of $^{11}Be + ^{12}C$

Results of calculation at energy 900 MeV are given in the file ***reac.out***, as shown in Table 4.4. Fig. 4.1 shows the energy dependence of the elastic and inelastic one-nucleon removal cross sections.

Table 4.4: *csc.inp* input file for **^{11}Be + ^{12}C** reaction system.

S/N	INPUT PARAMETERS	VALUES
1	Mass numbers of target, projectile and core: (A_T; A_P; A_C)	12, 11, 10
2	Atomic numbers of target, projectile and core: (Z_T; Z_P; Z_C)	6, 4, 4
3	Incident Energy per nucleon (in MeV)	900
4	Profile function parameters (σ_{NN}, α and β in fm^2)	4.17, -0.21, 0.200
5	l (angular momentum quantum number)	0
6	Monte Carlo parameters (Ns, δ, irand)	500000, 2.5, −11213
7	*icond1* (1:available, 0: not available)	0
8	Number of Gaussians used to fit the core and target densities	2
9	Coefficient c_i, range a_i (in fm^{-2}) of the Target	-1.25421 0.39907 1.39728 0.355553
10	Coefficient c_i range a_i (in fm^{-2}) of the Core	-1.22148, 0.413105 1.36161 0.361781

Table 4.5: wf.inp input file for **^{11}Be + ^{12}C** reaction system.

S/N	INPUT PARAMETERS	VALUES
1	Initial depth V_0 of the optical potential (in MeV)	70.0
2	Diffuseness parameter (in fm) a	0.6
3	Radius parameter r_0 (in fm)	1.2
4	Energy eigenvalue for the valence nucleon (in MeV)	-4.946
5	j value for the valence nucleon orbit	0.5
6	Node number for the valence nucleon orbit	1

Table 4.6: reac.out for the **^{11}Be + ^{12}C** reaction system at 900 MeV/nucleon projection energy.

S/no	Cross Section (in mb)	Result
1	Projectile reaction cross section	992.4
2	Core reaction cross section	852.7
3	Nucleon removal cross section	139
4	N-removal (elastic)	33.6
5	N-removal (Inelastic)	105.4

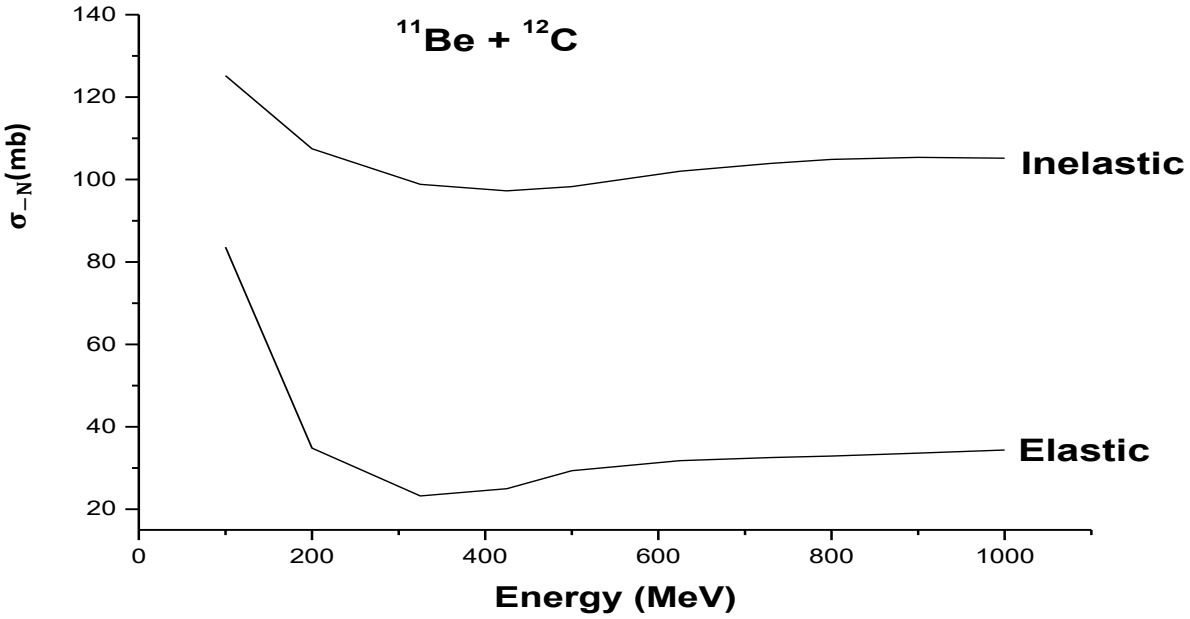

Figure 4.1: Energy dependence of the neutron-removal cross section for ^{11}Be+^{12}C system.

4.2.2.2 Reaction Cross Section of ^{19}C+ ^{12}C

The input parameter needed to fill in the input files csc.inp and wf.inp are shown in table 4.7. Results of calculation at energy 900 MeV are given in the file reac.out, in Table 4.8. In fact the rms radius of the neutron orbit becomes very large. Therefore ^{19}C is considered to be a good example for a one-neutron halo nucleus. Fig. 4.2 shows the energy dependence of the elastic and inelastic one-nucleon removal cross sections.

Table 4.7. *csc.inp* input file for **^{19}C + ^{12}C** reaction system.

S/N	INPUT PARAMETERS	VALUES
1	Mass numbers of target, projectile and core: (A_T; A_P; A_C)	12, 19, 18
2	Atomic numbers of target, projectile and core: (Z_T; Z_P; Z_C)	6, 6, 6
3	Incident Energy per nucleon (in MeV)	900
4	Profile function parameters (σ_{NN}, α and β in fm^2)	4.17, -0.21, 0.200
5	l (angular momentum quantum number)	0
6	Monte Carlo parameters (Ns, δ, irand)	500000, 2.5, −11213
7	*icond1* (1:available, 0: not available)	0
8	Number of Gaussians used to fit the core and target densities	2
9	Coefficient c_i, range a_i (in fm^{-2}) of the Target	-1.25421 0.39907 1.39728 0.355553
10	Coefficient c_i range a_i (in fm^{-2}) of the Core	-1.19721 0.300572 1.35334 0.255236

Table 4.8: reac.out for the **^{19}C + ^{12}C** reaction system at 900MeV/nucleon projection energy.

S/no	Cross Section (in mb)	Result
1	Projectile reaction cross section	1282.5
2	Core reaction cross section	1135.9
3	Nucleon removal cross section	147.3
4	N-removal (elastic)	36.8
5	N-removal (Inelastic)	110.4

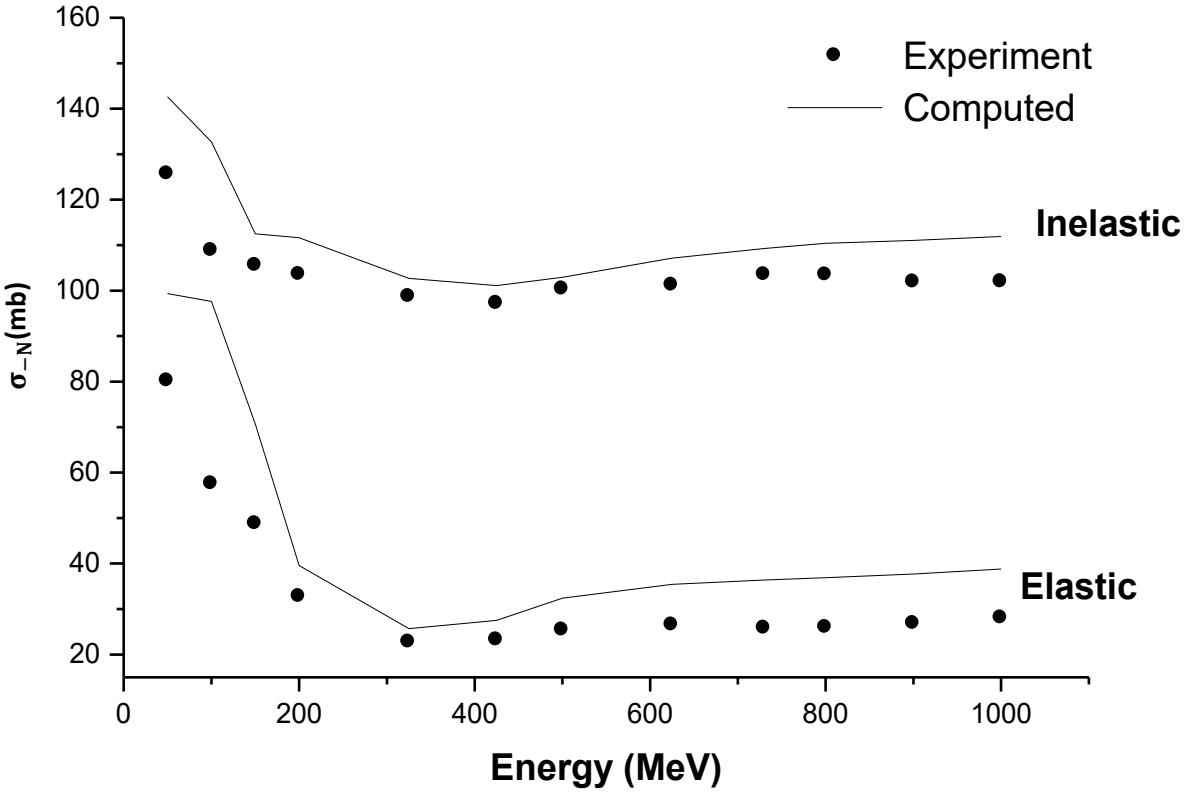

Figure 4.2: Energy dependence of the neutron-removal cross section for $^{19}C+^{12}C$ system. The experimental data is taken from (Panda and Patra, 2014).

4.2.2.3 Neutron-Removal Cross Section of $^{37}Mg + ^{12}C$

The input parameter needed to fill the input files csc.inp and wf.inp are shown in Tables 4.9 and 4.10. Fig. 4.3 shows the energy dependence of the elastic and inelastic one-nucleon removal cross sections.

Table 4.9: *csc.inp* input file for ^{37}**Mg +** ^{12}**C** reaction system.

S/N	INPUT PARAMETERS	VALUES
1	Mass numbers of target, projectile and core: (A_T; A_P; A_C)	12, 37, 36
2	Atomic numbers of target, projectile and core: (Z_T; Z_P; Z_C)	6, 12, 12
3	Incident Energy per nucleon (in MeV)	900
4	Profile function parameters (σ_{NN}, α and β in fm^2)	4.17, -0.21, 0.200
5	l (angular momentum quantum number)	0
6	Monte Carlo parameters (Ns, δ, irand)	500000, 2.5, −11213
7	*icond1* (1:available, 0: not available)	0
8	Number of Gaussians used to fit the core and target densities	2
9	Coefficient c_i, range a_i (in fm^{-2}) of the Target	-1.25421 0.39907 1.39728 0.355553
10	Coefficient c_i range a_i (in fm^{-2}) of the Core	-1.19721 0.300572 1.35334 0.255236

Table 4.10: wf.inp input file for ^{37}**Mg +** ^{12}**C** reaction system.

S/N	INPUT PARAMETERS	VALUES
1	Initial depth V_0 of the optical potential (in MeV)	42.0
2	Diffuseness parameter (in fm) a	3.5
3	Radius parameter r_0 (in fm)	1.2
4	Energy eigenvalue for the valence nucleon (in MeV)	-0.2201
5	j value for the valence nucleon orbit	0.5
6	Node number for the valence nucleon orbit	2

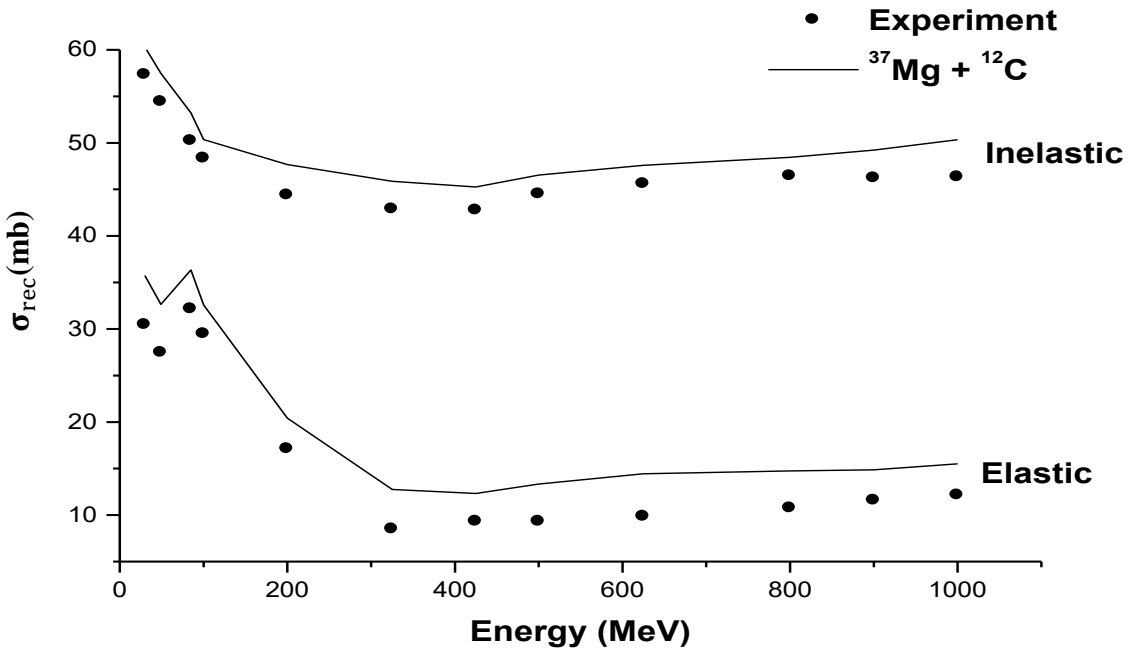

Figure 4.3: Energy dependence of the neutron-removal cross section for ^{37}Mg+^{12}C system. The experimental result is taken from (Sharma *et al.,* 2014).

4.2.3 One-Nucleon Removal from Total Reaction Cross Sections

Another evidence for the halo nature for these nuclei can be obtained from the projectile-target (P + T) and core-target (C + T) reaction cross sections as can be seen in the figures below.

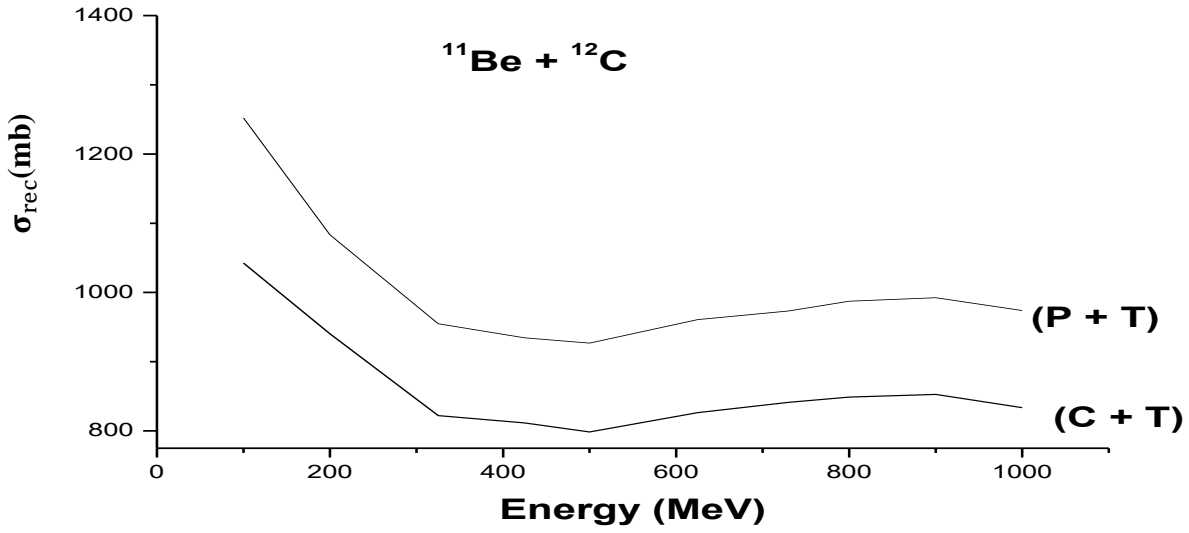

Figure 4.4: Energy dependence of (P + T) and (C + T) reaction cross section for ^{11}Be+^{12}C system

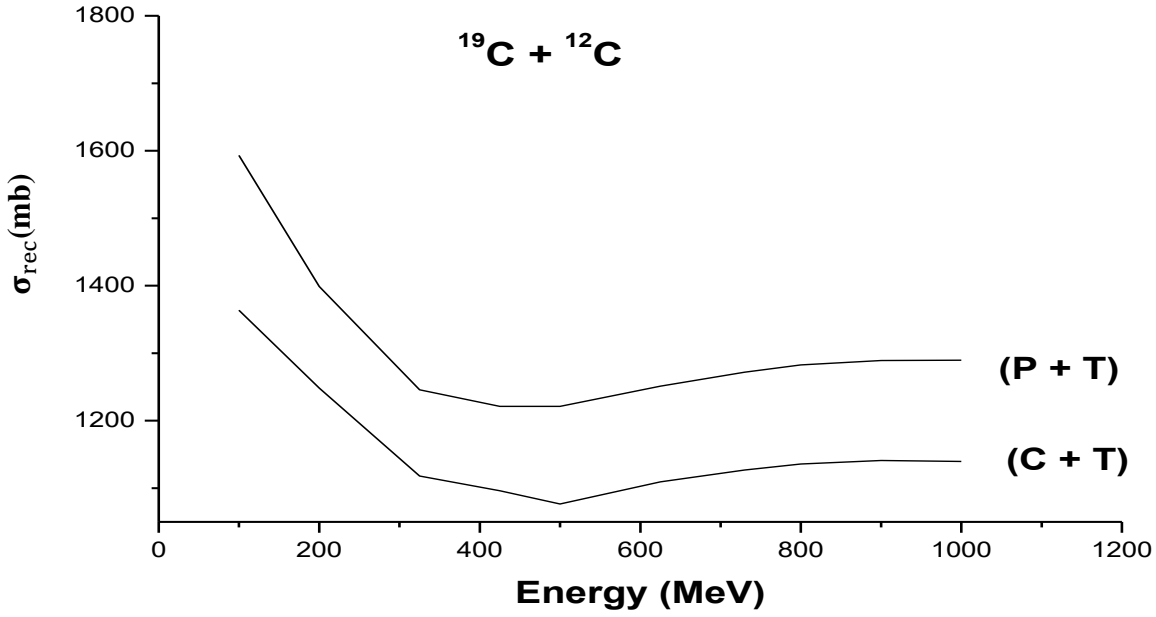

Figure 4.5: Energy dependence of (P + T) and (C + T) reaction cross section for ^{19}C+^{12}C system

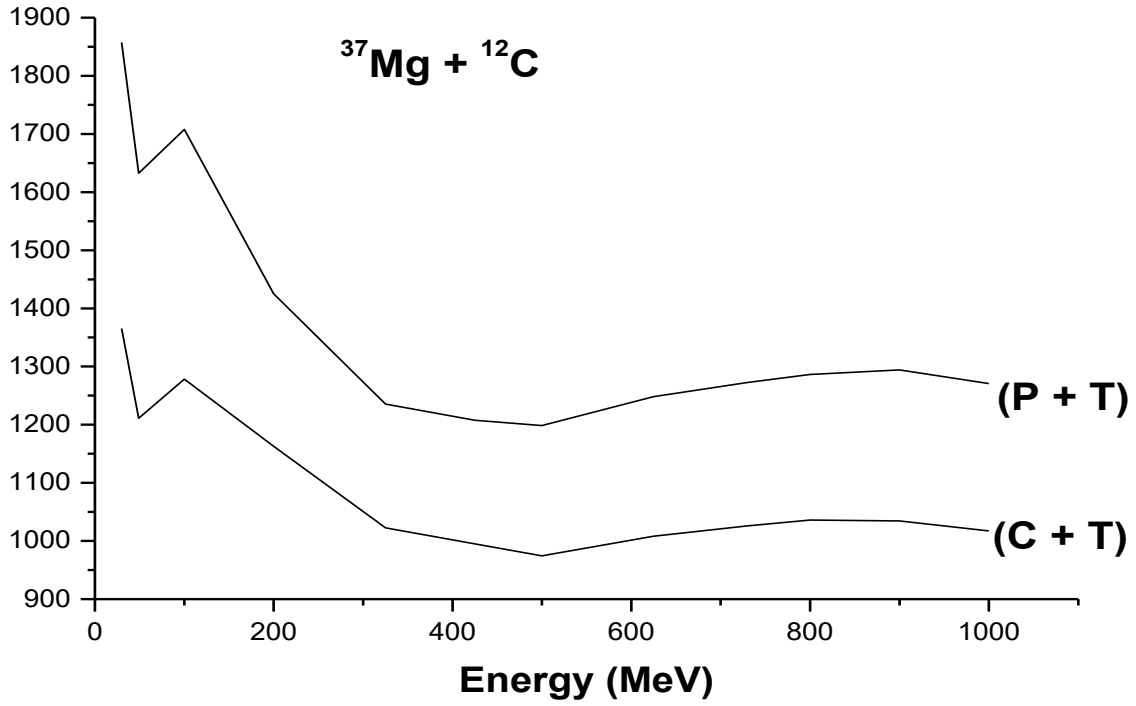

Figure 4.6: Energy dependence of (P + T) and (C + T) cross section for ^{19}C+^{12}C reaction system

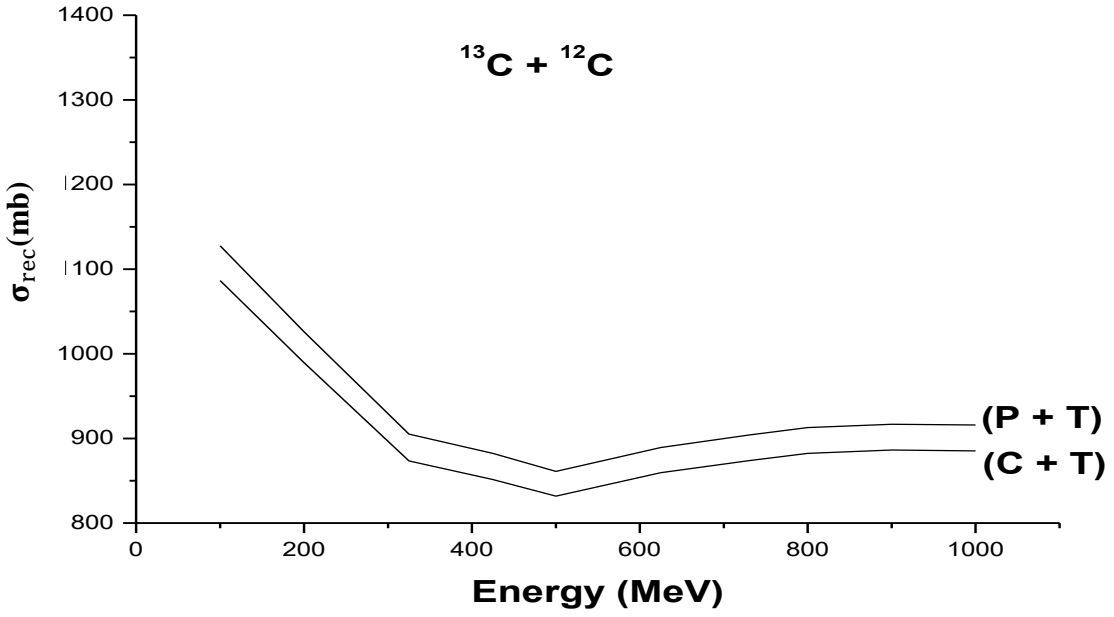

Figure4.7: Energy dependence of (P + T) and (C + T) cross section for ^{13}C+^{12}C reaction system.

4.3 GENERAL DISCUSSION

The results computed in this work includes the total reaction cross section, elastic and inelastic reaction cross section and one-nucleon removal cross section of ^{11}Be, ^{19}C and ^{37}Mg projectiles using ^{12}C as target. The ground states of ^{11}Be, ^{19}C and ^{37}Mg are assumed to be ^{10}Be, ^{18}C and ^{36}Mg plus one neutron systems respectively.

The computed total reaction cross sections of ^{11}Be, ^{19}C and ^{37}Mg, in Table 4.1, 4.2 and 4.3 respectively, indicates that the values calculated at high energies show an excellent agreement with the experimental results than those calculated at intermediate and low energies. This is exactly what is expected, as the superiority of the Glauber model that is mainly at high energy as indicated by the Glauber scattering amplitude Eqn. (2.28a). Note that at low energy the Glauber scattering amplitude reduce to Born approximation Eqn. (2.28b).

Figures 4.1, 4.2 and 4.3 are the energy dependence of one-nucleon removal cross section of these nuclei. It can be seen that, the one-nucleon removal cross section is large, reflecting their halo structures. The contribution from the inelastic breakup process is much larger than that from the elastic process in the energy region beyond a few hundred MeV per nucleon.

Figs 4.4, 4.5, 4.6 and 4.7 are the energy dependence of the (P + T) and (C +T) reaction cross section of ^{13}C, ^{11}Be, ^{19}C and ^{37}Mg nucleus. The gap between (P + T) and (C + T) for ^{11}Be, ^{19}C and ^{37}Mg are large compared to that of ^{13}C. The valence-neutron density is not spatially extended in ^{13}C, thus the difference between the reaction cross sections of (P + T) and (C + T) is not very large, indicating that ^{13}C is not a halo nucleus.

CHAPTER FIVE

SUMMARY, CONCLUSION AND RECOMMENDATIONS

5.1 SUMMARY

A Fortran program, CSC_GM was used to compute the total reaction and one-nucleon removal cross section of ^{10}Be, ^{12}C, ^{18}C and ^{36}Mg core fragments from ^{11}Be + ^{12}C, ^{13}C + ^{12}C, ^{19}C + ^{12}C and ^{37}Mg + ^{12}C reaction systems in the framework of the Glauber theory. The results obtained were compared with the available experimental results.

Total reaction cross sections for ^{11}Be + ^{12}C, ^{13}C + ^{12}C, ^{19}C + ^{12}C and ^{37}Mg + ^{12}C, reaction systems were computed at different energies using the CSC_GM code within the frame work of the Glauber Theory and the results compared well with experimental data. The results indicated that, the valence neutron in each nucleus is loosely coupled with the core containing all other nucleons and extended to a large distance.

The elastic and inelastic components of the one-nucleon removal cross sections of the above reaction system were also obtained. The high values of the one-nucleon removal cross section of ^{11}Be, ^{19}C and ^{37}Mg, indicates their halo structures. This brings the Glauber calculation closer to experiment.

For ^{13}C on the other hand the nucleon removal cross section is low, which indicate the high binding energy (4.946 MeV) for the valence nucleon. Also the difference between (P + T) and (C + T) is not very large, thus ^{13}C is not a halo nucleus.

Also the graphs of energy dependence of the elastic and inelastic components and the (P + T) and (C + T) to justify the halo nature of those nuclei were plotted.

One-nucleon removal cross section of ^{11}Be, ^{19}C, and ^{37}Mg at the energy range 30-1000MeV were computed. The results were plotted against energy as shown in Figures 4.1, 4.2, 4.3 and 4.4 respectively. Also the total projectile-target and core-target reaction cross sections of these nuclides were obtained at the same energy as above and the results are shown in Figures 4.4, 4.5, 4.6 and 4.7.

The code was originally run on Unix operating system, but in this work the code was modified and run on Linux operating system, which enable the computation of total and one-nucleon removal cross section of these nuclides. The result obtained indicated that ^{11}Be, ^{19}C and ^{37}Mg have a halo structures while ^{13}C does not show any halo characteristic.

5.2 CONCLUSION

The wide gap between the elastic and inelastic scattering cross sections in Figures 4.2 to 4.4 indicates high value of the one-nucleon removal cross section. The contribution from the inelastic breakup process is much larger than that from the elastic process in the energy region beyond a few hundred MeV per nucleon. The elastic breakup cross section is less than 30% of the total one-neutron removal cross section. The result shows that ^{11}Be, ^{19}C and ^{37}Mg are good examples of halo nuclei. For ^{13}C with low calculated nucleon removal cross section of (29.8mb at energy of 800MeV), shows no halo structure.

The agreement of these results with the experimental data justified the validity of CSC_GM used in the computation of nuclear reaction observables.

5.3 RECOMMENDATIONS

The Glauber model agrees very well with the experimental data at high energies. However, this Model fails to describe, reasonably, the collisions induced at relatively low energies. In such case it is recommended that the model should to be modified in order to take care of this problem. This would require further research in the topic beyond the scope of this work.

The CSC_GM code calculates nucleon removal cross section for only one-nucleon removal cross section. The code should, in further studies be modified to calculate multiple nucleon removal cross sections.

REFERENCES

Abu-Ibrahim, B., and Suzuki, Y. (2002). *Calculation of Nucleus* – Nucleus Cross Sections at Intermediate Energies Using Glauber Theory. *Nuclear Physics A 706, pp.111–122.*

Abu-Ibrahim, B. and Suzuki, Y. (2013). The optical potential of ^{6}He in the eikonal approximation. *American Physical Society journal. pp.2-7*

Adamu, I.D. (2013). Nuclear cross section calculations in the Glauber model. *Journal of Nigerian Association of Mathematical Physics,* **23,** pp.265-270,

Adamu, I. D. (2013). Calculation of Momentum Distributions of ^{7}Be Fragment From ^{8}B + ^{12}C Reaction Using The Glauber Theory. *IJRRAS* 17 (1), pp.116-121.

Al-Khalili, J. (2004). An Introduction to Halo Nuclei*, Lecture Notes on Physics. Springer-Verlag Berlin Heidelberg*. **651**, (77–112) pp 89–104.

Al-Khalili, J., and Nunes, F. (2003). Reaction Models to Probe The Structure of Light Exotic Nuclei. *Journal of Physics. G: Nucl. Part. Phys.* **29,** (R89–R132), pp.93–98.

Bertulani, C.A. and Gade, A. (2006). MOMDIS: Glauber Model Computer Code for Knockout Reactions. *Computer Physics Communications.* 175 372–380.

Bertsch, S. M. A. and G. F. (1995). Halo Nuclei. *Journal of American Physical Society*. pp.1-2

Byrd J. And Baertchy M. (2004). Numerical And Theoretical Treatment on Elastic Impacts Ionization. *American Physical Society , Four Coners Section Fall Meeting*. pp.15-16 .

El-Din, I. M. A. T., and Hassan, S. S. A. (2010). Study of Proton-Nucleus Total Reaction Cross Section at $30 \leq E_P \leq 2200$ Mev Using Relativistic Mean Field Densities. *Journal of Nuclear and Radiation Physics*, Vol. 5, No.1, pp. 40.

Esha, R. (2012). Glauber Modeling of High Energy. *National Institute of Science Education and Research Bhubaneswar*. Pp.1–2.

Fulmante, B. M., and Umashankar, S. (2013). Studies On Different Halo Nuclei Models. I*nternatonal Journal of Current Reseach and Academic Review 2*(3), Pp.169-173.

Gerjouy, E. and Thomas, B. K. (1974). Comparison of Eikonal-Born Series and Modified Glauber Approach for The Study of Elastic Electron by Hydrogen Scattering. *Springer Volume 13*, Pp89-95.

Glauber R.J., Brittin, W.E. and Dunham (Eds.) L.C., (1959). Lecture on Theoretical Physics, *Vol. 1, Interscience, New York,* p. 315.

Glauber R. J. (1969). Theory of High Energy Hardron-Nucleus Collision Review. *Presented at Third Int'n Conference on High Energy and Molecular Structure. Columbia University New York.*

Khyrallah G., (1976). Exchange Amplitudes For Electron-Hydrgen Scattering In The Glauber Theory. *Physical Review A (General Physics)* 14, pp. 2064-2070

Kobayashi, N., Nakamura, T., Kondo, Y., Tostevin, J. A., Utsuno, Y., Aoi, N., and Yoneda, K. (2014). Observation of a *p* -Wave One-Neutron Halo Configuration in Mg. *ReseachGate 16*(68), pp.1-5.

Mahesh K. Sharma, Manoj K. Sharma, R. N. Panda & S. K. Patra (2015). Quest of ^{37}Mg Halo Structure Using Glauber Model and Microscopic Relativistic Mean Field Densities. *Journal of American Physical Society* . Pp. 4-6

Miller, M. L., Reygers, K., Sanders, S. J., and Steinberg, P. (2007). Glauber Modeling in High Energy Nuclear Collisions. *Annual Review Nuclear and particle*

Ogawa, Y., Suzuki, Y. and Tanihata, I. (2003). Cross Section Calculations In Glauber Model : I . Core Plus One-Nucleon Case. *Computer Communication Physics, (02) 151. pp. 369–386.*

Ozawa, A., Suzuki, T., & Tanihata, I. (2001). Nuclear Size And Related Topics. Nuclear Physics A 693 40 Pp.32–62.

Panda, R., N. and Patra, S., K. (2010). Structure Effect on One Neutron Removal Reaction Using Relativistic Mean Field Densities In Glauber Model. *Journals of American Physical Society 21. Pp1-7.*

Riley K.F., Hobson M.P. and Bence S. J., (2006). Mathematical Methods For Physics And Engineering Third Edition. *Cambridge University Press*. Pp750-753

Sauvan E., Carstoiu, F., Orr, N. A., Winfield, J. S., Freer, M., Ang´elique, J. C., Catford, W. N., Clarke, N. M., Mac Cormick, M., Curtis, N., Gr´evy, S., Le Brun, C., Lewitowicz, M., Li´egard, E., Marqu´es, F. M., Roussel-Chomaz, P., Saint Laurent, M.G., and Shawcross, M. (2003). One-neutron removal reactions on light neutron-rich nuclei. *Phys Rev. C69. arXiv:nucl-ex/0307019v2 29 pp.1-9.*

Sawhney, G., Sharma, M. K. and Gupta, R. K. (2014). Neutron-Halo Structure Of Light Nuclei Studied With Effects Of Deformations, *055101, 2–3. Doi:10.1088/0954-3899/41/5/055101*

Sharma, M. K., Panda, R. N., Sharma, M. K., and Patra, S. K. (2013). Reaction and Structure Effects Of Light Mass Nuclei Using Glauber Model With Relativistic and Non Relativistic Effective Interaction Densities. Journal of American Physical Society 25. Pp. 8–9.

Sharma, M. K., Sharma, M. K. and Patra, S. K. (2013). Reaction Dynamics For Some Halo Nuclear Systems Using Glauber Model With Relativistic Mean Field Densities. *APS Journals -American Physical Society 58. Pp.461.*

Shubhchintak, Neelam, R. Chatterjee, R. Shyam and K. Tsushima (2015). Coulomb Breakup Of ^{37}Mg and Its Ground State Structure, arXiv:1501.03642v2. Pp.14-16.

Shukla, A., Sharma, B. K., Chandra, R., Arumugam, P. and Patra, S. K. (2014). Nuclear Reaction Studies Of Unstable Nuclei Using Relativistic Mean Field Formalisms In Conjunction With Glauber Model. *APS Journals, 6,: 21.10.-k, 21.10.dr, 21.10.Ft, 21.30.-x, 24.10.-1, 24.10.Jv.*

Tanihata, I. (1996). Neutron Halo Nuclei. *Journal of Physics. G: Nucl. Part. Phys. 22, 157-198.*

Tanihata, I. (1995). Nuclear Structure Studies from Reaction Induced by Radioactive Nuclear Beams. *Progress in Particle and Nuclear Physics.* Vol. 35, Pp. 505-573.

Tanihata, I., Savajols, H. and Rituparna K. (2013). Recent experimental progress in nuclear halo structure studies. *Journal Progress in Particle and Nuclear Physics,* vol. 68, pp.215–313.

Wallace S. J. (1973). Multiple scattering eikonal expansion systematic correction to the Glauber theory. *Reseachgate*. vol. 8, pp.1846-1863.

Wilkin C. (1968). nuclear and particle physcics .*(new york: benjamin*)

Yahiro, M., Ogata, K., Matsumoto, T., and Minomo, K. (2012). The Continuum Discretized Coupled-Channels. *IOSR Journals,* Vol, *206*, pp.1–44.